ARTICLES
https://doi.org/10.1038/s42255-021-00487-4
nature metabolism

Serine catabolism generates liver NADPH and supports hepatic lipogenesis

Zhaoyue Zhang[1,2,5], Tara TeSlaa[2,5], Xincheng Xu[1,2], Xianfeng Zeng[1,2], Lifeng Yang[2], Gang Xing[3], Gregory J. Tesz[3], Michelle F. Clasquin[3] and Joshua D. Rabinowitz[1,2,4] ✉

Carbohydrate can be converted into fat by de novo lipogenesis, a process upregulated in fatty liver disease. Chemically, de novo lipogenesis involves polymerization and reduction of acetyl-CoA, using NADPH as the electron donor. The feedstocks used to generate acetyl-CoA and NADPH in lipogenic tissues remain, however, unclear. Here we show using stable isotope tracing in mice that de novo lipogenesis in adipose is supported by glucose and its catabolism via the pentose phosphate pathway to make NADPH. The liver, in contrast, derives acetyl-CoA for lipogenesis from acetate and lactate, and NADPH from folate-mediated serine catabolism. Such NADPH generation involves the cytosolic serine pathway in liver running in the opposite direction to that observed in most tissues and tumours, with NADPH made by the SHMT1–MTHFD1–ALDH1L1 reaction sequence. SHMT inhibition decreases hepatic lipogenesis. Thus, liver folate metabolism is distinctively wired to support cytosolic NADPH production and lipogenesis. More generally, while the same enzymes are involved in fat synthesis in liver and adipose, different substrates are used, opening the door to tissue-specific pharmacological interventions.

Lipids function as both structural molecules and energy storage in living cells. The main long-term energy store in mammals is triglycerides: fatty acids esterified to a glycerol backbone. To store ingested carbohydrates or protein as triglycerides, it is necessary to convert them into fatty acids. This occurs via the process of de novo lipogenesis[1].

Diverse disease processes are associated with increased de novo lipogenesis, including viral infection[2,3], cancer[4,5] and non-alcoholic fatty liver disease (NAFLD)[6,7]. Yet, the quantitative contribution of different nutrients to the acetyl-CoA and NADPH pools that support lipogenesis remains unclear.

De novo lipogenesis polymerizes acetyl-CoA molecules into fatty-acid chains using the reducing power of NADPH. Acetyl-CoA can be produced from carbohydrate via pyruvate dehydrogenase in the mitochondria, from acetate in the cytosol and from fatty acids and amino acids in mitochondria or peroxisomes. Lipogenesis, however, requires cytosolic acetyl-CoA. Mitochondrial acetyl-CoA can be transferred to the cytosol by first generating mitochondrial citrate which is then trafficked to the cytosol and converted into acetyl-CoA by ATP citrate lyase.

Isotope tracing into fatty acids provides a readout of the nutrient sources feeding into cytosolic acetyl-CoA. Such studies have illuminated complexities in carbohydrate conversion into fat. For example, fructose, a highly lipogenic carbohydrate, contributes to liver lipogenesis indirectly via microbiome-derived acetate[8–10]. Whether other nutrients, such as glucose, contribute to lipogenesis directly or indirectly via other circulating substrates such as lactate, and whether this varies across tissues, remains an open question.

The canonical cytosolic NADPH production route is the oxidative pentose phosphate pathway (oxPPP) and accounts for the bulk of NADPH production in cultured cancer cells and T cells[11–13]. Other cytosolic NADPH enzymes include malic enzyme (ME1), isocitrate dehydrogenase 1 (IDH1) and methylene tetrahydrofolate dehydrogenase 1 (MTHFD1) and 10-formyltetrahydrofolate dehydrogenase in folate metabolism[14,15]. Quantitative measurements of the sources of NADPH production for lipogenesis have not previously been made in vivo.

Here we use ^{2}H-stable-isotope-tracer technology to track NADPH production in vivo and employ it together with ^{13}C tracing to determine the circulating sources of the tissue acetyl-CoA and NADPH used for lipogenesis. We find that circulating glucose provides both acetyl-CoA and NADPH for lipogenesis in brown adipose tissue. In contrast, the liver uses circulating acetate and lactate to make acetyl-CoA, and folate-mediated serine catabolism to generate NADPH. Genetic or pharmacological inhibition of folate-mediated serine catabolism suppresses hepatic lipogenesis.

Results

Lipogenesis is a substantial source of saturated fat. Fatty acids can either be derived from diet or be synthesized from other nutrients by de novo lipogenesis. Those that can be synthesized by de novo lipogenesis are called non-essential. Two non-essential fatty acids are highly abundant in mammals: palmitate (C16:0; 16 carbons and zero double bonds) and oleate (C18:1). Together with the essential fatty acid linoleate (C18:2)[16], these 3 fatty acids account for roughly 80% of body fat[17] (Extended Data Fig. 1a,b). We sought to determine whether lipogenesis accounts for a meaningful fraction of tissue fatty acids and in which tissues lipogenic flux occurs.

To quantify the fraction of tissue fat from lipogenesis in mice fed standard carbohydrate-rich lab chow, we used isotope-labelled water (20% D_2O)[18–23]. Drinking of labelled water did not perturb mouse body weight (Extended Data Fig. 1c). Deuterium from heavy water is stably incorporated into newly synthesized fatty acids both directly and via NADPH[24]. Serum labelling of saponified fatty acids, which reflects both free fatty acids and those covalently embedded in phospholipids and triglycerides, reached steady state with a half time of around 1 week; white adipose tissue (WAT) reaches steady state more slowly (Extended Data Fig. 1d). At steady state,

[1]Department of Chemistry, Princeton University, Princeton, NJ, USA. [2]Lewis-Sigler Institute for Integrative Genomics, Princeton University, Princeton, NJ, USA. [3]Pfizer Inc. Internal Medicine, Cambridge, MA, USA. [4]Ludwig Institute for Cancer Research, Princeton Branch, Princeton University, Princeton, NJ, USA. [5]These authors contributed equally: Zhaoyue Zhang, Tara TeSlaa. ✉e-mail: joshr@princeton.edu

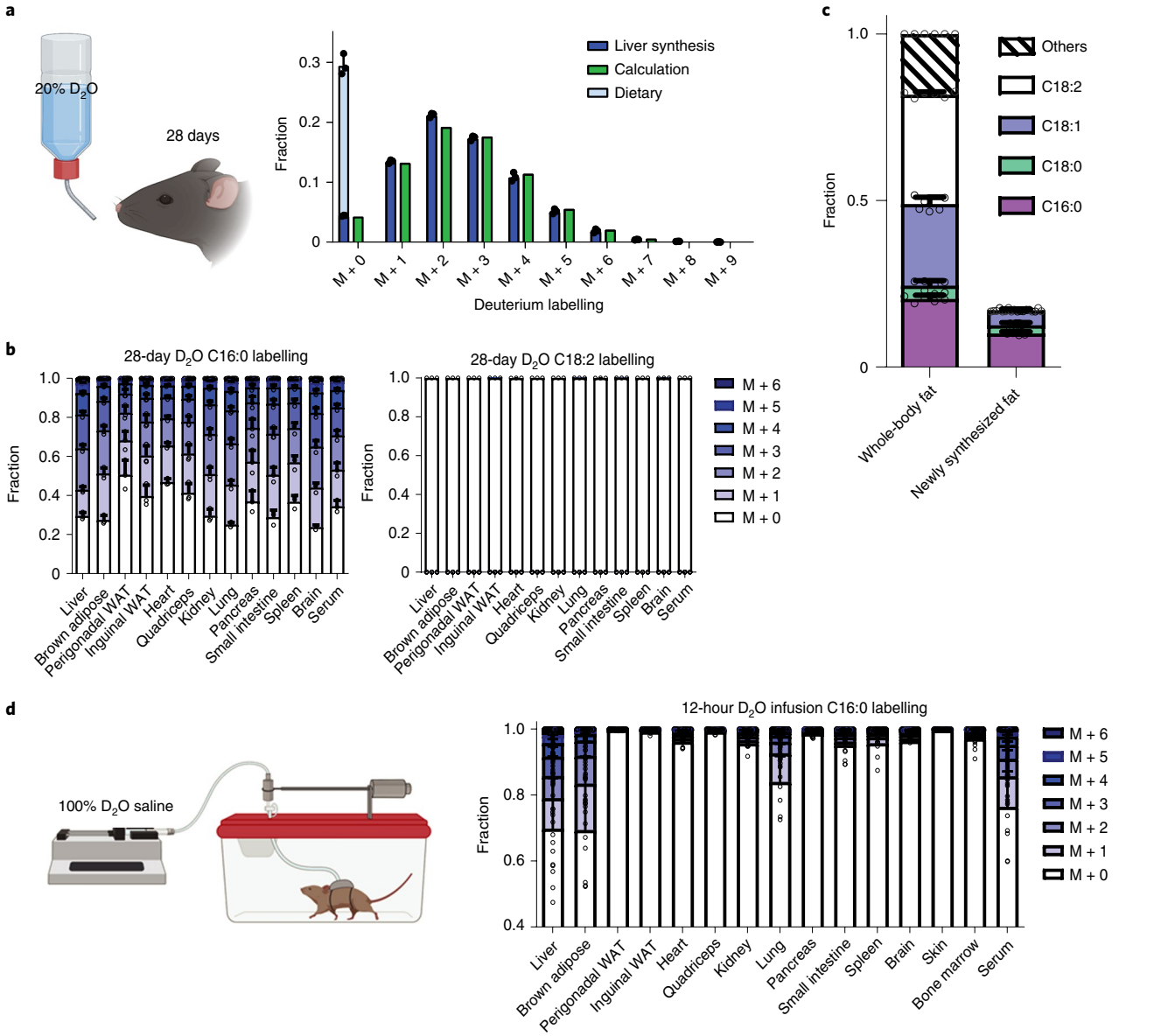

Fig. 1 | De novo lipogenesis in liver and brown adipose produces much of whole-body saturated fat. a, Liver palmitate (C16:0) labelling pattern after 4 weeks of D_2O drinking. Left bars (blue) reflect the experimentally observed labelling; right bars (green) reflect the calculated labelling based on the fraction of newly synthesized fat and observed D_2O and NADPH labelling. The fraction of dietary versus synthesized fat is based on fitting the labelling pattern. Throughout the paper, all data are for saponified fatty acids. **b**, Palmitate (C16:0) and linoleate (C18:2) labelling pattern across tissues after 4 weeks D_2O drinking. C18:2 is an essential fatty acid and accordingly shows no labelling. **c**, Composition of whole-body fat (left) and fraction that is endogenously synthesized based on the 4-week D_2O drinking data (right). **d**, C16:0 labelling pattern across tissues after 12-hour fed-state D_2O infusion. Mean ± s.d., $n = 6$ mice for composition analysis (3 males and 3 females); $n = 3$ males for D_2O drinking experiment and $n = 10$ (5 males and 5 females) for 12-hour D_2O infusion. Images in **a** and **d** were created with BioRender.com.

the fraction of each fatty acid coming from synthesis, as opposed to diet, was determined by fitting the observed mass isotopic distribution (Fig. 1a). Labelling of saponified palmitate was extensive across serum and all tissues, while, as expected, linoleate was completely unlabelled (Fig. 1b). Quantitative analysis, summing de novo fatty-acid amounts across tissues, revealed that most fatty acids (~80%) in mice come from diet[25], but in mice fed standard carbohydrate-rich (62.1% calorie) chow, about half of saturated fat is synthesized de novo (Fig. 1c).

A challenge in interpreting long-term D_2O labelling experiments is that fat can be exchanged between organs, and indeed, the steady-state measurements revealed nearly indistinguishable palmitate labelling across tissues (Fig. 1b and Extended Data Fig. 1e). To elucidate the organs responsible for lipogenesis, we performed 6- to 12-hour intravenous infusions of D_2O[26], which provide sufficient enrichment to detect labelling in both NADPH and palmitate with minimal stress to the animal, and during which D_2O enrichment increased linearly (Extended Data Fig. 1g). Measurements taken throughout the day at 6-hour intervals confirmed that lipogenesis in mice occurs more rapidly at night, when mice are more active and eat more (Extended Data Fig. 1h). Overnight infusions showed greatest saponified-fatty-acid labelling in liver and brown adipose tissue (Fig. 1d and Extended Data Fig. 1i,j), consistent with liver's canonical lipogenic role and brown adipose lipogenesis

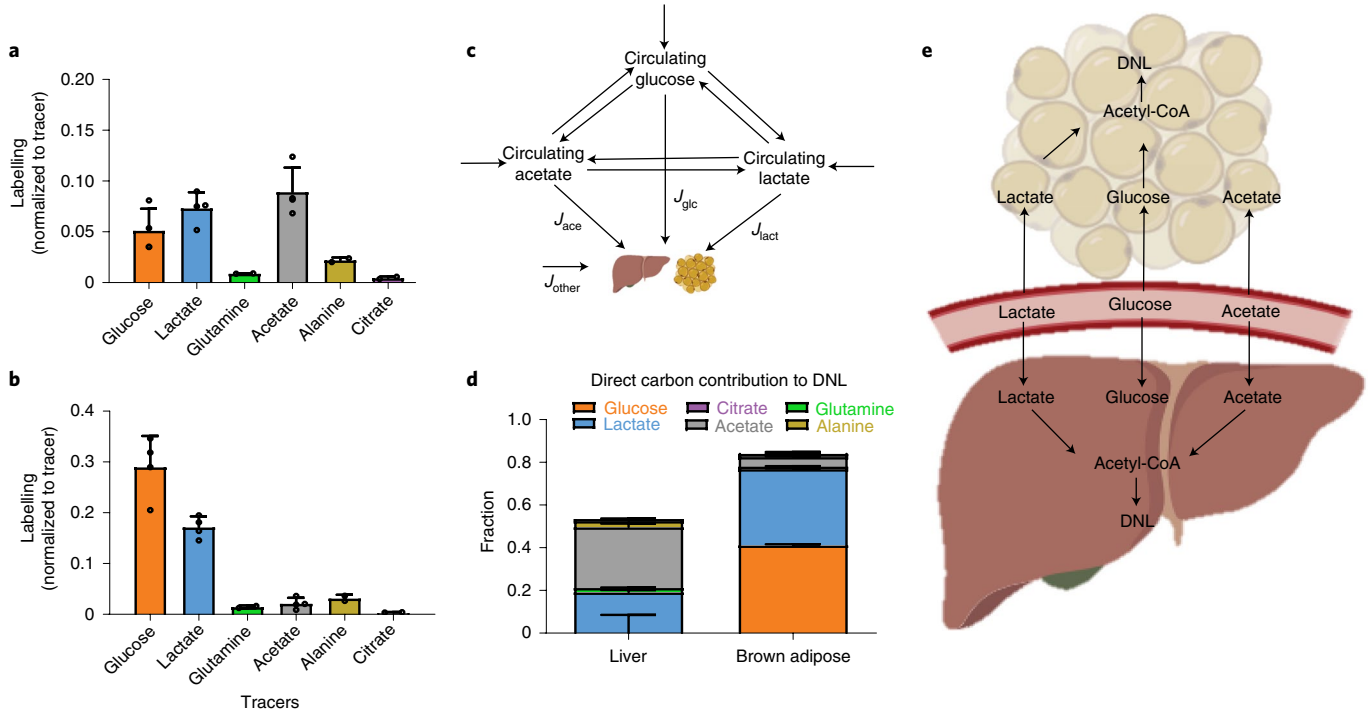

Fig. 2 | Liver and brown adipose use different carbon sources to support lipogenesis. a, Average atom labelling of liver C16:0 following 12-hour infusion of [U-^{13}C]glucose ($n = 4$), [U-^{13}C]lactate ($n = 4$), [U-^{13}C]glutamine ($n = 2$), [U-^{13}C]acetate ($n = 4$), [U-^{13}C]alanine ($n = 2$) and [U-^{13}C]citrate ($n = 2$). Labelling is normalized to circulating tracer labelling. Brown adipose is perfused by systemic blood (approximated by tail vein sampling) and liver by 78% portal vein blood and 22% systemic blood. **b**, As in **a**, for brown adipose C16:0. **c**, Isotope tracing into fat is complicated by interconversion of the tracer with other circulating metabolites. By conducting tracer experiments with all key circulating substrates, the direct contribution of each can be determined by linear algebra. **d**, Carbon sources supporting de novo lipogenesis in liver and brown adipose, based on direct contributions to C16:0, calculated using data in **a** and **b** and Extended Data Fig. 2f. **e**, Schematic of differential lipogenic substrate use by liver versus brown adipose. Data in **a** and **b** are mean ± s.d.; data in **d** are mean ± s.e.m. All mice are males. Results in females are similar (Extended Data Fig. 6). Images in **c** and **e** were created with BioRender.com.

induction in mice housed at room temperature[27]. Only in these two tissues did labelling exceed that of circulating fat (Fig. 1d and Extended Data Fig. 1i,j). This does not rule out the possibility of de novo synthesis in other tissues such as white adipose, in which slow fractional labelling can occur owing to the large pre-existing fat pool (indeed, refeeding after fasting for 24 hours increased fat labelling from D_2O in white adipose tissue but not liver or brown adipose[28], Extended Data Fig. 1k). Nevertheless, these data unambiguously show that liver and brown adipose tissue can actively engage in de novo lipogenesis.

Liver and adipose use different substrates to make fat. Next, we focused on identifying the carbon sources supporting palmitate synthesis in liver and brown adipose. To this end, we infused various ^{13}C-labelled nutrients and monitored circulating nutrient and saponified tissue palmitate labelling. ^{13}C-Tracers were infused at rates that did not substantially elevate the infused metabolite's levels (Extended Data Fig. 2a–c and Methods). In the circulation, labelling was observed in both the infused tracer and downstream metabolites. To account for dilution of tracer by absorbed food, serum samples were collected from both the tail vein and the portal vein that carries blood from the intestine to the liver (Extended Data Fig. 2d,e). Palmitate was labelled from both glucose and lactate in both the liver and brown adipose, whereas labelling from acetate was prominent only in the liver (Fig. 2a,b and Extended Data Fig. 2f).

The relative labelling from glucose and lactate differed between liver and brown adipose, with lactate labelling more fatty acid in liver and glucose labelling more in adipose (Fig. 2a,b). Because glucose and lactate interconvert via glycolysis and gluconeogenesis, infusion of either substrate labels both in the circulation[26] (Fig. 2c and Extended Data Fig. 2d,e). Accordingly, even if only one of the substrates is used by a tissue to drive lipogenesis, we will observe labelling from infusion of either substrate. By monitoring the extent of tissue palmitate labelling from infusion of each substrate, as well as the extent of cross-labelling between the substrates, the direct contribution of each substrate can be determined. Specifically, in each tracer experiment, the observed fat labelling reflects the sum of each substrate's direct fat contribution multiplied by its circulating labelling. The resulting equations can be solved for each substrate's direct contribution by a linear-algebra calculation[26,29]. This analysis revealed that, although glucose and lactate both directly contribute to brown adipose lipogenesis, glucose contributes indirectly to hepatic lipogenesis through circulating lactate (Fig. 2d,e)[26,30]. Importantly, there is no discernible direct circulating glucose contribution to liver fat synthesis (Fig. 2d). Consistent with this, lactate but not glucose contributed to TCA cycle intermediates in liver tissue slices (Extended Data Fig. 3). Collectively, these findings support lactate (the classical liver gluconeogenic substrate[31,32]) and acetate (the substrate of the prolipogenic and cancer-supporting enzyme ACSS2[33–37]) as being primary lipogenic inputs to liver.

NADPH in brown adipose comes from the oxPPP. Much of the energy in fatty acids comes from NADPH[1], which donates hydrogen to drive acetyl reduction. The canonical cytosolic NADPH production route is the oxidative pentose phosphate pathway (oxPPP)[1,38,39]. To investigate whether NADPH produced by the oxPPP supports hepatic lipogenesis, we began by studying cultured primary hepatocytes. Hepatocytes (both in liver and primary cells in culture) only weakly express oxPPP enzymes[40]. OxPPP flux can be measured in vitro by monitoring the differential $^{14}CO_2$ release from [1-^{14}C]

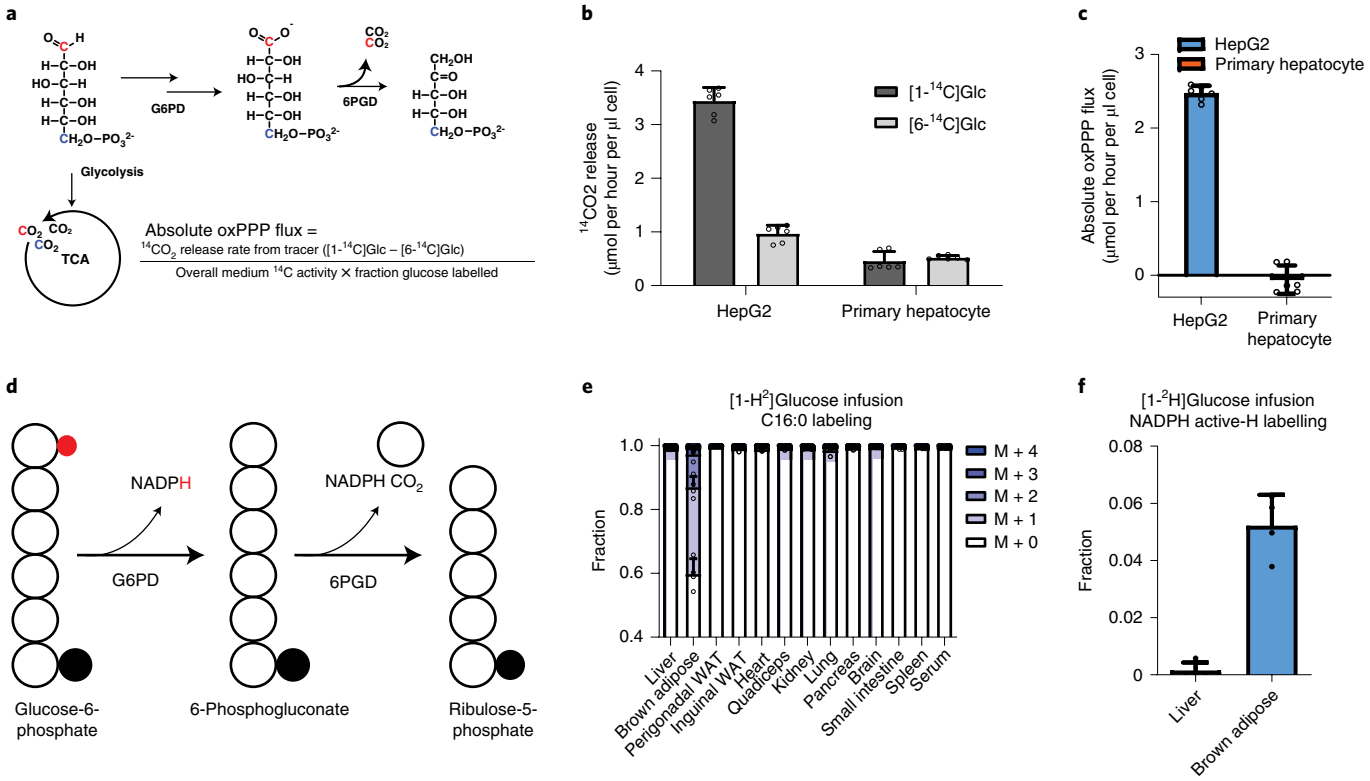

Fig. 3 | Brown adipose, but not liver, generates lipogenic NADPH via the oxPPP. a, Scheme for ^{14}C experiment to examine absolute oxPPP flux. **b**, $^{14}CO_2$ release flux from [1-^{14}C]glucose and [6-^{14}C]glucose in HepG2 and primary hepatocytes. **c**, Absolute oxPPP flux in HepG2 and primary hepatocytes. **d**, Schematic of the pathway by which [1-^{2}H]glucose labels NADPH via the oxPPP. **e**, C16:0 labelling across tissues following 12-hour [1-^{2}H]glucose infusion (125 nmol per minute per g body weight). **f**, NADPH active-H measurement in liver and brown adipose from 12-hour [1-^{2}H]glucose infusion (125 nmol per minute per g body weight). Mean ± s.d., $n = 6$ replicates for cultured cell experiments; $n = 4$ mice for [1-^{2}H]glucose infusion. All mice are males. Results in females are similar (Extended Data Fig. 6).

glucose (oxPPP tracer) and [6-^{14}C]glucose. The two tracers produce $^{14}CO_2$ identically when glucose is catabolized in the TCA cycle, with greater $^{14}CO_2$ release from [1- ^{14}C]glucose quantitatively reflecting oxPPP flux (Fig. 3a). Hepatocellular carcinoma cells (HepG2) manifested strong oxPPP flux, as expected for cancer cells, but the absolute oxPPP flux in primary mouse hepatocytes was undetectable (Fig. 3b,c).

Flux from the oxPPP can also be traced into NADPH's redox-active hydrogen using glucose deuterated at C1 or C3 (Fig. 3d). Such labelling can be read out in NADPH itself or in downstream products, such as newly synthesized fatty acids. In prior work in cultured cancer cells, we found that NADPH deuterium labelling from the oxPPP is incomplete owing to Flavin-enzyme-mediated exchange of NADPH's active hydrogen with water[14,24]. Correcting for such exchange, which can be monitored using D_2O, revealed that the oxPPP is the main cytosolic NADPH source in most cultured cancer cells[11,39,41]. Whether non-transformed lipogenic cells mainly use the oxPPP to generate NAPDH remains unclear. Using [3-^{2}H]glucose we found that, unlike HepG2 cells, primary hepatocytes manifest almost no NADPH and fat labelling from oxPPP, suggesting the predominance of alternative NADPH production pathways[15] (Extended Data Fig. 4a–e).

We next translated the ^{2}H-tracing technology in vivo by infusing mice with [1-^{2}H]glucose overnight. We observed strong labelling of brown adipose palmitate (Fig. 3e), confirming the effectiveness of this tracing strategy. After correcting for the fraction of NADPH's active hydrogen that is exchanged with water and the extent of tissue glucose labelling (Fig. 3e and Extended Data Fig. 4f), we found that the oxPPP accounts for nearly all cytosolic brown fat NADPH production (Fig. 4f right). Liver fat was not labelled, however, indicating that liver relies on alternative NADPH sources (Fig. 3e,f). These results agree with negligible expression of *G6pd* in hepatocytes, and its greater expression in brown adipose, white adipose and leukocytes, including liver-resident T cells and Kupffer cells[42–46]. Thus, the oxPPP is the main source of brown adipose NADPH.

Hepatocytes prefer glutamine for TCA only in vitro. Multiple studies have identified isocitrate dehydrogenase 1 (IDH1) and malic enzyme 1 (ME1) as important cytosolic NADPH producers in lipogenic cells[15,47,48]. Consistent with this, lysates of primary hepatocytes showed substantial ME1, and especially IDH1, activity (Extended Data Fig. 4d). In addition, [2,3,3,4,4-^{2}H]glutamine labelled the redox-active hydrogen of NADPH and downstream fat in primary hepatocytes, reflecting cytosolic NADPH production from ME1 and/or IDH1 (Extended Data Fig. 4a,b). After correcting for hydrogen–deuterium exchange on the basis of experiments with D_2O, the combined contribution of the oxPPP, malic enzyme and IDH in primary hepatocytes was, however, less than 50% (Extended Data Fig. 4e).

To determine whether IDH1 and ME1 are major sources of liver NADPH in vivo, we attempted [2,3,3,4,4-^{2}H]glutamine infusion. Unfortunately, there was extensive deuterium loss between glutamine and malate/isocitrate, rendering the resulting lack of labelling in palmitate uninformative (Extended Data Fig. 4i–k). To determine why [2,3,3,4,4-^{2}H]glutamine tracing was successful in cultured hepatocytes but not in vivo, we performed [U-^{13}C]glutamine tracing to analyse the TCA cycle. We found that glutamine is the predominant hepatocyte TCA substrate in vitro but not in vivo[49]

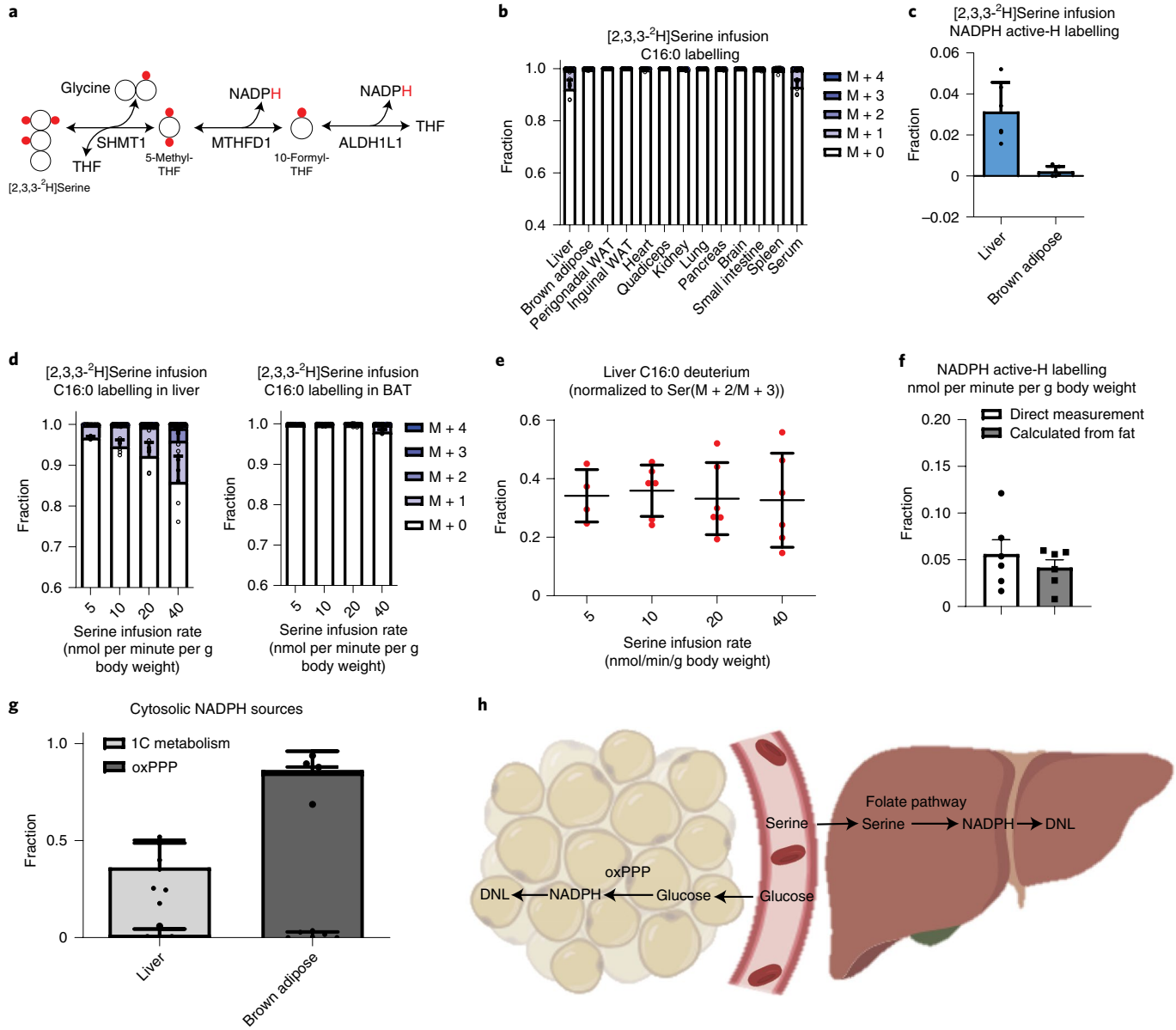

Fig. 4 | Serine's hydride contribution to liver fat across an eightfold range of [2,3,3-^{2}H]serine infusion rates. a, Schematic of pathway by which [2,3,3-^{2}H]serine labels NADPH via cytosolic folate metabolism. **b**, C16:0 labelling across tissues following 12 h [2,3,3-^{2}H]serine infusion (20 nmol per minute per g body weight). **c**, NADPH active-H measurement in liver and brown adipose from 12 h [2,3,3-^{2}H]serine infusion (20 nmol per minute per g body weight). **d**, Liver and brown adipose tissue C16:0 labelling following 12-hour [2,3,3-^{2}H]serine infusion at different rates, ranging from minimally to highly perturbative. **e**, Corresponding normalized contribution of serine to liver C16:0 hydrogen (average number of labelled hydrogens in C16:0 relative to fraction serine $M + 2$ or $M + 3$). **f**, NADPH active-H labelling following 12-hour [2,3,3-^{2}H]serine infusion at 40 nmol per minute per g body weight, measured either directly (from Extended Data Fig. 5f) or calculated from palmitate (from Fig. 4d left). **g**, Hydride sources supporting de novo lipogenesis in liver and brown adipose, correcting for substrate labelling and H–D exchange between NADPH and water. Calculated on the basis of tracer data in **c** and **f** and D_2O exchange data in Extended Data Fig. 4f. **h**, Schematic of differential lipogenic substrate use by liver versus brown adipose. All data are mean ± s.d., $n = 4$ for 5 nmol per minute per g body weight and $n = 6$ for 10, 20 and 40 nmol per minute per g body weight of [2,3,3-^{2}H]serine infusion. All mice are males. Panel **h** was created with BioRender.com.

(Extended Data Fig. 4h). Alternative approaches to label the relevant hydrogen atoms of malate and isocitrate were unsuccessful, even in cultured hepatocytes (Extended Data Fig. 4l).

Serine catabolism feeds liver NADPH production. The above findings suggest that the oxPPP, malic enzyme and IDH collectively account for no more than half of cytosolic NADPH production in primary hepatocytes. Serine catabolism is a potential alternative NADPH source, which drives mitochondrial NADPH production for redox defence during cancer metastasis[50]. So far, however, serine catabolism has not been shown to be a physiologically relevant contributor to cytosolic NADPH. We explored whether serine might contribute to NADPH production in primary hepatocytes using [2,3,3-^{2}H]serine (Fig. 4a). In cultured hepatocytes, we observed NADPH and downstream fat labelling from [2,3,3-^{2}H]serine (Extended Data Fig. 4a,b,e).

We next turned our attention to whether serine contributes to NADPH production in the liver in vivo. Infusion of [2,3,3-^{2}H]serine

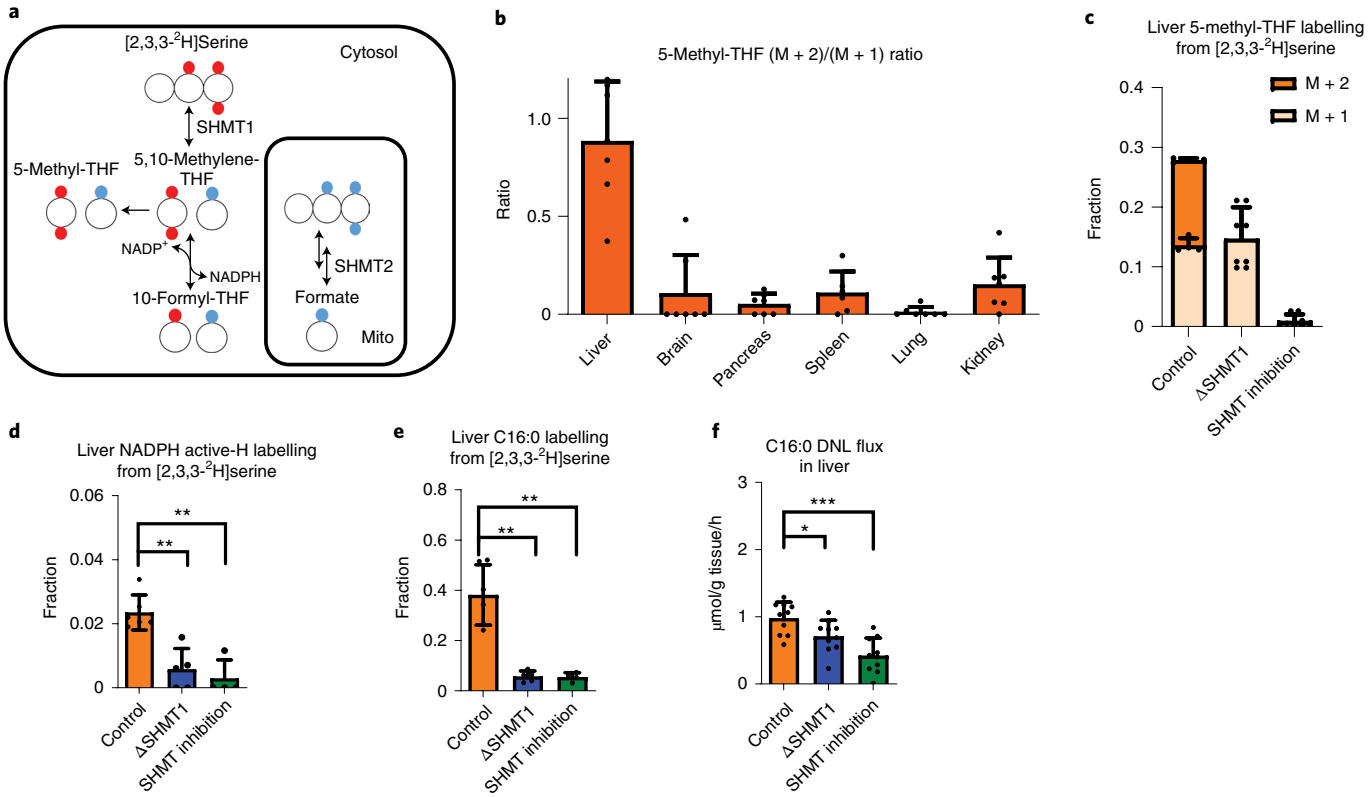

Fig. 5 | Liver serine catabolism generates NADPH via SHMT1–MTHFD1–ALDH1L1 and thereby supports hepatic lipogenesis. a, Schematic of the cytosolic and mitochondrial serine catabolic pathways. Metabolite labelling from [2,3,3-^{2}H]serine generated by the cytosolic pathway is shown in red, and from the mitochondrial pathway in blue. **b**, 5-Methyl-THF labelling for 12-hour [2,3,3-^{2}H]serine infusion (20 nmol per minute per g body weight). The ratio of $M+2$ to $M+1$ labelling reflects relative contribution of cytosolic versus mitochondrial serine catabolism to 1C units in 5-methyl-THF. **c**, 5-Methyl-THF labelling in liver for 12-hour [2,3,3-^{2}H]serine infusion (20 nmol per minute per g body weight) in control, whole-body SHMT1-knockout (ΔSHMT1) mice, and mice treated with the dual SHMT1/2 inhibitor SHIN2 (3.33 mg kg^{-1} h^{-1} i.v. infusion). **d**, NADPH active-H measurement in liver for 12-hour [2,3,3-^{2}H] serine infusion (20 nmol per minute per g body weight) (control versus ΔSHMT1, $P = 0.0048$; control versus SHIN2 treatment, $P = 0.0043$). **e**, C16:0 labelling in liver for 12-hour [2,3,3-^{2}H]serine infusion (20 nmol per minute per g body weight). Labelling is normalized to liver serine enrichment and reported as the average number of labelled hydrogens in C16:0 (control versus ΔSHMT1, $P = 0.0043$; control versus SHIN2 treatment, $P = 0.0095$). **f**, C16:0 lipogenesis flux in liver overnight, as measured by 12-hour D_2O infusion (control versus ΔSHMT1, $P = 0.043$; control versus SHIN2 treatment, $P = 0.0002$). Mean ± s.d. For serine tracing, $n = 6$ for control, $n = 5$ for ΔSHMT1, $n = 4$ for inhibitor treatment. For D_2O infusion in **f**, $n = 10$ for all three conditions. All mice are males. $^*P < 0.05$, $^{**}P < 0.01$; $^{***}P < 0.005$ by unpaired Mann–Whitney test, all P values are two-sided.

at 20 nmol per minute per g body weight did not detectably label palmitate in brown fat (Fig. 4b), nor did it label liver acetyl-CoA or related liver metabolites (Extended Data Fig. 5b). Impressively, however, we obtained substantial labelling in NADPH's active hydrogen and palmitate in the liver (Fig. 4b,c).

As serine catabolism had not been previously established as a physiological NADPH source, to assess the robustness of serine's hepatic NADPH contribution, we replicated the ^{2}H-serine infusion across an eightfold range of rates (from 5 to 40 nmol per minute per g body weight). The lowest infusion rates were minimally perturbative, and the highest rates increased serum serine concentration by twofold but resulted in enough labelling that we could more readily analyse downstream metabolites (Extended Data Fig. 5a,c–f). In brown fat, palmitate labelling from ^{2}H-serine was minimal even at the highest infusion rate. In contrast, in liver, labelling was detected across all infusion rates in direct proportionality to the administration rate of labelled serine (Fig. 4d). The observed labelling in liver reflects a consistent normalized contribution from [2,3,3-^{2}H]serine to hepatic fat (Fig. 4e). The highest serine infusion rate (40 nmol per minute per g body weight) led to substantial labelling in both fat and NADPH's redox-active hydrogen, with the extent of NADPH and fat labelling in quantitative agreement (Fig. 4f). The carbon and hydride contributions of different substrates to fat, including serine's NADPH contribution, were consistent across male and female mice (Extended Data Fig. 6). Thus, serine provides hydride to NADPH that contributes to liver lipogenesis (Fig. 4g,h).

The SHMT1–MTHFD1–ALDH1L1 folate pathway makes liver NADPH. We hypothesized that the pathway linking serine to NADPH and liver fat synthesis is folate-mediated cytosolic serine catabolism via the SHMT1–MTHFD1–ALDH1L1 reaction sequence[14]. Both MTHFD1 and ALDH1L1 are capable of making NADPH, although neither had been shown to do so in a physiological context[51]. Indeed, in most cells, MTHFD1 runs in the NADPH-consuming direction[52]. To assess the direction of one-carbon flux in vivo, following [2,3,3-^{2}H]serine infusion, we monitored the labelling of 5-methyl-tetrahydrofolate (5-methyl-THF). Serine catabolism in mitochondria, followed by reassimilation of the resulting formate in the cytosol, results in $M + 1$ 5-methyl-THF and consumes cytosolic NADPH. In contrast, cytosolic serine catabolism generates $M + 2$ 5-methyl-THF and can support cytosolic NADPH production[53] (Fig. 5a). We observed a predominance of $M + 1$ 5-methyl-THF in most tissues, with a strong $M + 2$ 5-methyl-THF signal, indicative

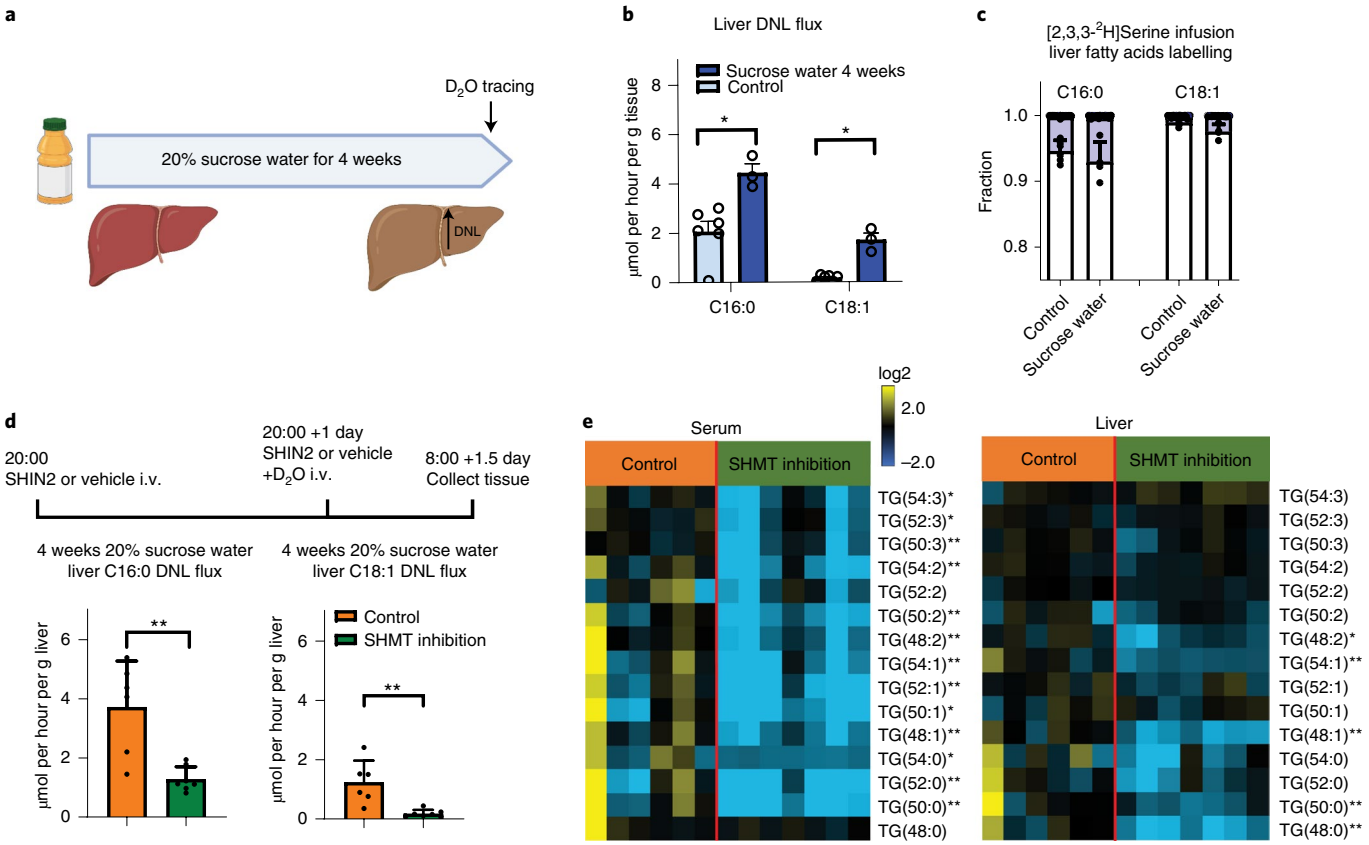

Fig. 6 | Sucrose-induced lipogenesis consumes hydride from serine and depends on SHMT activity. a, C16:0 and C18:1 lipogenesis flux in liver of control mice and mice given 20% sucrose water for 4 weeks (control versus sucrose water drinking, $P = 0.024$ for liver C16:0, $P = 0.024$ for liver C18:1). **b**, C16:0 and C18:1 labelling from 12-hour [2,3,3-^{2}H]serine infusion (10 nmol per minute per g body weight) in control mice and mice given 20% sucrose water for 4 weeks. **c**, Impact of pharmacological SHMT1/2 inhibition on sucrose-induced lipogenesis. Mice were given 20% sucrose in the drinking water for 4 weeks. Then, 36 hours before euthanization and tissue collection, they were given vehicle or SHIN2 (3.33 mg kg^{-1} h^{-1} i.v. infusion). The SHIN2 or vehicle infusion was then augmented by D_2O infusion for the final 12 hours, which corresponded to the fed state (nighttime). Lipogenesis with or without SHIN2 treatment is shown (control versus SHIN2 treatment, $P = 0.0047$ for C16:0; $P = 0.0023$ for C18:1). **d**, Serum and hepatic triglyceride (TG) levels with or without SHIN2 treatment, in heatmap format. (Control versus SHIN2 treatment, for serum, TG(48:0) $P = 0.23$, TG(50:0) $P = 0.0012$, TG(52:0) $P = 0.0047$, TG(54:0) $P = 0.0221$, TG(48:1) $P = 0.0023$, TG(50:1) $P = 0.014$, TG(52:1) $P = 0.0047$, TG(54:1) $P = 0.0082$, TG(48:2) $P = 0.0012$, TG(50:2) $P = 0.0023$, TG(52:2) $P = 0.29$, TG(54:2) $P = 0.0082$, TG(50:3) $P = 0.0082$, TG(52:3) $P = 0.035$, TG(54:3) $P = 0.014$. For liver, TG(48:0) $P = 0.0012$, TG(50:0) $P = 0.0082$, TG(52:0) $P = 0.051$, TG(54:0) $P = 0.051$, TG(48:1) $P = 0.0012$, TG(50:1) $P = 0.94$, TG(52:1) $P = 0.14$, TG(54:1) $P = 0.0012$, TG(48:2) $P = 0.014$, TG(50:2) $P = 0.53$, TG(52:2) $P = 0.073$, TG(54:2) $P = 0.23$, TG(50:3) $P = 0.14$, TG(52:3) $P = 0.63$, TG(54:3) $P = 0.051$.) Mean ± s.d. For experiments comparing control mice and mice given sucrose water, $n = 6$ for control, $n = 3$ for mice given sucrose water. For experiments comparing vehicle to SHIN2 treatment, $n = 6$ for control and $n = 7$ for SHIN2 treatment. *$P < 0.05$; **$P < 0.01$; ***$P < 0.005$ by unpaired Mann–Whitney test, all statistics values are two-sided. All mice are males. Panel **a** was created with BioRender.com.

of SHMT1-mediated cytosolic serine catabolism, specifically in liver (Fig. 5b and Extended Data Fig. 7a).

To confirm that the observed NADPH and fatty-acid labelling in liver is derived from cytosolic serine catabolism, we carried out [2,3,3-^{2}H]serine tracing in *Shmt1* whole-body knock-out mice, which are viable, fertile and exhibit no major metabolic defects[51,54] (Extended Data Fig. 7b). As expected, these mice showed a complete loss of *M*+2 5-methyl-THF (Fig. 5c). We also observed an 80% drop in NADPH and palmitate labelling from ^{2}H-serine in the liver (Fig. 5d,e and Extended Data Fig. 7c,d,g). Thus, SHMT1-driven serine catabolism is a substantial NADPH source for hepatic lipogenesis.

In the absence of SHMT1, folate metabolism can contribute to hepatic NADPH production via ALDH1L1, which oxidizes 10-formyl-THF[55]. Serine can contribute to cytosolic formyl-THF either via SHMT1–MTHFD1 or via the mitochondrial enzymes SHMT2–MTHFD2–MTHFD1L[56–58]. To probe the importance of ALDH1L1, we carried out tracer studies with [^{2}H]formate, and we observed substantial NADPH and fat labelling, although less than that from deuterated serine (Extended Data Fig. 7e,f). Thus, both the SHMT1–MTHFD1 reaction sequence, and downstream ALDH1L1, which can also be fed via the SHMT2 pathway, contribute to serine-driven hepatic NADPH production.

To more completely inhibit serine's hepatic NADPH contribution, we used a pharmacological dual SHMT1/2 inhibitor, SHIN2[53]. Treatment with SHIN2 markedly decreased both NADPH and palmitate labelling from [2,3,3-^{2}H]serine in liver (Fig. 5d,e). Labelling from [^{2}H]formate, which feeds directly into the formyl-THF pool[55] and can generate cytosolic NADPH via ALDH1L1, was maintained (Extended Data Fig. 7f).

Inhibition of serine catabolism decreases liver lipogenesis. Finally, we assessed whether manipulation of serine-driven NADPH production could impact the overall rate of hepatic lipogenesis. D_2O tracing revealed that both *Shmt1* knockout and pharmacological SHMT1/2 inhibition significantly decreased hepatic

but not brown adipose fat synthesis (Fig. 5f and Extended Data Fig. 8a–g). Decreased lipogenesis in response to SHMT1/2 inhibition was observed regardless of the route of D_2O delivery (intravenous or intraperitoneal) (Extended Data Fig. 8c,d). Consistent with liver making circulating fat, *Shmt1* knockout decreased serum fat labelling from both [2,3,3-^{2}H]serine and D_2O. Labelling in some other tissues (for example, lung and bone marrow) also decreased, probably because they acquire fat originally made in the liver from the circulation (Extended Data Figs. 7g and 8h). Perhaps owing to compartmentation and/or measurement imprecision, we did not detect a statistically significant impact of *Shmt1* knockout or SHMT1/2 inhibition on overall tissue NADPH, serine or glutathione, but we did observe an increased oxidized:reduced glutathione ratio in response to SHMT1/2 inhibition (Extended Data Fig. 8i–n). During refeeding after fasting, liver lipogenic flux was also decreased in the *Shmt1*-knockout mice (Extended Data Fig. 8o). Collectively, these data indicate that inhibition of serine catabolism decreases hepatic lipogenesis.

To determine whether there is compensation from other NADPH sources, we used the oxPPP tracer [1-^{2}H]glucose in the *Shmt1* knockout mice but did not observe fat labelling in liver (Extended Data Fig. 9a). Thus, SHMT1 loss does not induce liver oxPPP activity. Furthermore, we did not observe changes in expression of other lipogenic and NADPH-producing enzymes, such as malic enzyme (Extended Data Fig. 9b,c).

Rates of de novo lipogenesis increase in fatty liver disease and in response to diets high in sugar (fructose or sucrose)[6,8,59–61]. Therefore, we analysed the role of liver SHMT1–MTHFD1–ALDH1L1 in lipogenesis induced by drinking water containing sucrose, mimicking human soda consumption (Fig. 6a scheme). After 4 weeks of water with 20% sucrose, lipogenesis flux increased significantly in liver but not in brown adipose tissue (Fig. 6b and Extended Data Fig. 10a,b). The enhanced hepatic lipogenesis resulted in increased serum fat labelling, which exceeded brown adipose fat labelling, making it infeasible to quantify local brown fat lipogenesis rate or inputs in this condition, as the observed labelling could be coming from uptake of circulating fat (Extended Data Fig. 10b). Lipogenesis in the liver, however, still utilized NADPH produced by serine catabolism (Fig. 6c).

Finally, we examined whether sucrose-induced liver lipogenesis could be mitigated by inhibition of serine catabolism. After extended sucrose water drinking, we administered the SHMT1/2 inhibitor SHIN2 IV for 36 hours (Fig. 6d scheme). D_2O infusion during the last 12 hours of the inhibitor treatment revealed a significant decrease in hepatic lipogenesis[62] (Extended Data Fig. 10c and Fig. 6d). Consistent with this, in both liver and serum, we also observed decreased levels of triglyceride species containing saturated fatty acids (Fig. 6e). Moreover, circulating saponified fatty acids (palmitate, oleate), decreased (Extended Data Fig. 10d).

Discussion

The past century of biochemical research has revealed the enzymatic network of metabolism in exquisite detail. Yet the way that these enzymes work together within and across different tissues remains less fully defined. For de novo lipogenesis, despite its medical importance, the upstream precursors had not been quantitatively assessed. Using stable isotope tracing, we found that circulating glucose supplies both carbon and hydride for lipogenesis in brown adipose tissue. In the liver, however, other substrates were used for both roles, with serine catabolism emerging as an unexpected cytosolic NADPH source.

Serine catabolism through one-carbon metabolism is important for organismal development, cancer cell growth and immune function[63–66]. The enzymes important for these functions are, however, mitochondrial (for example SHMT2, MTHFD2, and MTHFD1L)[50,52,54,67,68], with the physiological function of cytosolic SHMT1 being a long-standing puzzle[54]. The present data show that, although most tissues generate one carbon units from serine via the mitochondrial pathway, the liver uniquely relies on cytosolic serine catabolism. Flux running from serine through SHMT1–MTHFD1–ALDH1L1 generates a net of two NADPH per serine, which support hepatic lipogenesis. Our flux measurements align with enzyme expression data, with SHMT1, MTHFD1 and ALDH1L1 all highly expressed in liver. Moreover, expression of the mitochondrial serine catabolic enzymes MTHFD2 and MTHFD1L is low in the liver[40]. This precludes flux in liver from mitochondrial serine catabolism to cytosolic 10-formyl-THF, and thereby favours coupled cytosolic formyl-THF and NADPH production via SHMT1–MTHFD1. Together with low liver glucose-6-phosphate dehydrogenase expression and oxPPP flux, these data suggest a primary role of gene expression in controlling in vivo NADPH production routes. This unique directionality of hepatic one-carbon metabolism may be related to the liver's redox requirements for drug detoxification, cholesterol production and de novo lipogenesis.

To measure de novo lipogenesis, a standard methodology is tracking passage of deuterium from deuterated water into fat. Typically, this is done by oral or intraperitoneal administration of deuterated water[69–71]. Here, however, we also used intravenous infusion. In animals that can receive intravenous injections, this allows delivery of a large volume of D_2O in a temporally controlled manner without the animal handling (and potential associated stress-induced alterations in lipogenesis) associated with intraperitoneal dosing[70,72–74]. The resulting increased deuterium labelling enabled label detection directly in NADPH, in addition to in fat[24].

De novo lipogenesis is a target of interest for treating cancer[75] and non-alcoholic fatty liver disease[76]. To date, drug-development efforts have focused on the core fatty-acid biosynthetic enzymes, acetyl-CoA carboxylase (ACC1) and fatty acid synthase (FASN)[76], which are required for fat synthesis across all tissue types and tumours. ACC1 inhibitors have proven effective in decreasing lipogenesis but cause hypertriglyceridemia in both rodents and humans[77,78]. Although the mechanism underlying the hypertriglyceridemia remains unclear, a concern with general lipogenesis inhibition is that excess carbon must ultimately be safely stored.

The physiological location for long-term carbon storage is adipose[79,80]. Accordingly, it is conceptually appealing to selectively block lipogenesis in the liver or in tumours, while retaining adipose lipogenesis. The present data show that, despite *Acss2* being widely expressed[40], acetate is a liver-specific lipogenic carbon source. Moreover, serine catabolism is a liver-specific cytosolic NADPH source. The associated dependency of hepatic but not adipose lipogenesis on ACSS2 and SHMT1 offers a potential strategy to inhibit preferentially hepatic lipogenesis. Further work is merited to assess the risks and benefits of this approach in relevant disease states.

Methods

Mouse experiments. Mouse work was approved by the Princeton University Institute Animal Care and Use Committee (protocol no. 2032). Mice were housed under a normal light cycle (lights on 8:00–20:00) and were fed a standard chow diet, PicoLab Rodent 20 (Lab Diet, cat. no. 5053), ad libitum unless otherwise noted. The standard chow contains 5% fat by weight (1% saturated fat), while a typical Western diet contains 21% fat by weight (13% saturated fat). Eight-week-old wild-type C57BL/6NCrl mice were purchased from Charles River Laboratories (strain code no. 027). Mice were allowed at least 5 days[81] of acclimation to the facilities prior to experiments, and were randomly chosen for different experimental conditions. No blinding was implemented. Drinking water, 20% deuterium water (Cambridge Isotopes, cat. no. DLM-6) and 20% sucrose water (Sigma Aldrich, cat. no. 84097) experiments started 1 week after arrival and lasted for 4 weeks or more, with tail vein blood collected weekly for circulating fatty acid labelling. For experiments involving 24 hours of fasting, food was removed at 20:00 and replaced at 20:00 + 1 day, followed by refeeding with tracing.

Intravenous tracer infusions were done on mice after in-house right jugular vein catheterization. During infusions, mice are single housed and can move freely in the cage with normal access to food and water. Mice were 10–16 weeks old at the time of isotope infusion measurements. Unless otherwise indicated, infusions were

performed during the dark cycle from 20:00 to 8:00 + 1 day, during which time the mice are more active, feed more and synthesize more fat. All tracers were dissolved in 0.9% saline. Tracer concentrations and infusion rates are shown in Table 1.

Tail blood was collected via tail snip prior to euthanization to measure circulating labelling. Blood samples were kept on ice to coagulate and then were centrifuged at 4 °C to separate serum. Thereafter, mice were anaesthetised with isoflurane, opened and resected. The portal vein was cut, and portal blood was taken with a pipet. Then, 12 tissues were collected in the following order: liver, spleen, pancreas, kidney, small intestine, perigonadal white adipose tissue, inguinal white adipose tissue, quadriceps, lung, heart, brown adipose tissue and brain. All tissues were immediately clamped with a liquid nitrogen temperature Wollenberger clamp and dropped in liquid nitrogen. After tissue collection, mice were euthanized by cervical dislocation.

For intraperitoneal D_2O injections for measurement of de novo lipogenic flux, 33 µl per gram body weight of D_2O saline (0.9% NaCl) was injected at 20:00, and mice were provided drinking water with 5% deuterium water to maintain enrichment throughout the experiment. At 8:00 + 1 day, serum was collected via tail snip, mice were anaesthetised with isoflurane and tissues were collected as described above. Mice were single housed for a week prior to the experiment, and were between 10 and 16 weeks of age at the time that the experiment was performed.

***Shmt1* knockout mice and pharmacological SHMT inhibition.** The whole-body *Shmt1* knockout mice were a generous gift from P. J. Stover[54] and were bred at Princeton for more than ten generations as heterozygotes on the C57Bl/6 background. Homozygotes knockout progeny and littermate wild-type control mice were used in experiments. For SHMT1/2 inhibition experiments, the small molecule SHMT inhibitor SHIN2 was dissolved in 20% 2-hydroxypropyl-β-cyclodextrin as a 20 mg ml^{-1} stock and diluted in 0.9% saline to the desired concentration. Drug or vehicle control was intravenously infused, sometimes together with tracers, through the jugular vein catheter at an infusion rate of 3.33 mg kg^{-1} h^{-1}, which is equivalent to 40 mg per kg SHIN2 over a 12-hour period.

Primary hepatocyte collection and cell culture. Primary hepatocytes were isolated from wild-type C57BL/6 mice[82] and cultured in high glucose (4.5 g/L) DMEM medium supplemented with 1% penicillin–streptomycin, 100 nM insulin, 100 nM dexamethasone and 1% glutamax. Primary hepatocytes were cultured in collagen-coated six-well plates in a 37 °C, 5% CO_2 incubator. HepG2 cells were obtained from ATCC (ATCC HB-8065) and cultured in DMEM with 10% FBS. For labelling experiments, primary hepatocytes were isolated, cultured overnight and used the next morning. For isotope labelling experiments, HepG2 cells were changed into the same condition as primary hepatocytes 24 hours prior to the start of tracing. Medium was aspirated and replaced with otherwise identical prewarmed medium containing the indicated isotope tracer in place of the corresponding unlabelled nutrient. The duration of labelling was 2.5 hours for soluble metabolite measurement and 6 hours for fat measurement. To collect metabolites, medium was aspirated and 500 µl, −20 °C 40:40:20 methanol:acetonitrile:water with 0.5% formic acid was directly added, and then neutralized immediately with 15% NH_4HCO_3 solution (2.2% vol/vol of extraction buffer). Cells were collected with a scraper and transferred together with extraction buffer into a 1.5 ml vial on dry ice. Samples were incubated on dry ice for 1–1.5 hours, then thawed on ice and centrifuged at 4 °C and 16,000*g* for 10 minutes. Supernatant was then directly analysed by liquid chromatography–mass spectrometry.

Table 1 | Tracer infusion parameters

Tracer	Concentration	Infusion rate (µl per minute per g body weight)	Infusion flux (nmol per minute per g body weight)
D_2O	100%	0.2	
[2,3,3-^{2}H]Serine	400 mM	0.1	40
	200 mM		20
	100 mM		10
	50 mM		5
[1-^{2}H]Glucose	625 mM	0.2	125
[2,3,3,4,4-^{2}H]Glutamine	150 mM	0.2	30
[U-^{2}H]Formate	80 mM	0.1	8
[U^{13}C]Glucose	400 mM	0.2	80
[U^{13}C]Sodium lactate	5% w/w	0.1	45
[U^{13}C]Sodium acetate	150 mM	0.1	15
[U^{13}C]Glutamine	170 mM	0.1	17
[U^{13}C]Alanine	300 mM	0.1	30
[U^{13}C]Citrate	20 mM	0.1	2

Liver slice experiments. Wild-type C57BL/6 mice were anaesthetised with isoflurane. Livers were resected and liver tissue slices from different lobes were collected with combined two blades and immediately transferred into six-well plates with Krebs–Ringer buffer (with 10 mM glucose, 3 mM sodium lactate, 0.8 mM sodium acetate and 1 µM insulin) with the metabolites replaced by labelled forms as indicated. Then the slices were cultured in an incubator at 37 °C, 5% CO_2 for 2 hours or 6 hours. Thereafter, tissue slices were washed with ice-cold PBS, frozen on dry ice, ground and metabolites extracted.

Enzymatic activity assays. A diaphorase-resazurin-coupled biochemical assay was used to detect G6PD, IDH1 and ME1 enzyme activity in cell lysates. Cytosolic proteins were isolated by subcellular protein fractionation kit (Thermo, 78840). Then 2% vol/vol of cytosolic lysate was mixed with buffer (50 mM Tris pH 7.4, 5 mM $MgCl_2$, 1 mM resazurin, 0.25 mM $NADP^+$, 0.1 U ml^{-1} diaphorase and 0.1 mg ml^{-1} BSA). To this mixture, substrate (glucose-6-phosphate for G6PD, isocitrate for IDH1 and malate for ME1) was added to a final concentration of 1 mM to initiate reactions. The kinetics of NADPH production were recorded by relative fluorescent unit measurement using a plate reader. The excitation wavelength was 540 nm and emission wavelength 590 nm.

Radioactive CO_2 release from oxPPP pathway. $^{14}CO_2$ release from [1-^{14}C]glucose and [6-^{14}C]glucose was used to measure oxPPP flux as previously described[11,14]. Briefly, cells were grown in rubber-stopper-sealed tissue culture flasks with DMEM containing 0.5 µCi ml^{-1} [1-^{14}C]glucose or [6-^{14}C]glucose. Then 150 µl of 10 M KOH was added to a centre well (Kimble Chase) containing a piece of filter paper. After 16 hours, cell metabolism was quenched, and CO_2 was released by injecting 1 ml 3 M acetic acid through the stopper. Everything in the centre well was transferred into a scintillation vial for counting. Absolute flux was calculated as previously described[11,14].

qRT–PCR protocol. Liver tissue was weighed out and RNA isolated with TRIzol reagent (Life Technologies); 1 ml of TRIzol reagent was used per 50 mg of tissue and RNA was extracted according to the manufacturer's instructions. RNA was converted to complementary DNA with iScript (Bio-Rad). Quantitative reverse transcription–PCR (qRT–PCR) was performed with ViiA 7 system using Fast SYBR green (Applied Biosystems). Primers were generated as custom DNA oligonucleotides from Integrated DNA Technologies (IDT), and sequences were either from Roche Universal library or taken from the literature as indicated in Supplementary Table 1 (ref. [77]). All data were normalized to the expression of ribosomal protein lateral stalk subunit P0 (*Rplp0*) as a control.

LC–MS sample preparation. Tissue samples were stored at ≤−70 °C. Tissues were pulverized using a Cryomill (Retsch); 10–20 mg of the resulting powder was weighed into a precooled tube for extraction.

Soluble metabolites extraction was done by adding −20 °C 40:40:20 methanol:acetonitrile:water with 0.5% formic acid to the resulting powder (40 µl solvent per mg tissue) and the samples were first vortexed for 5 seconds and then neutralized immediately with 15% NH_4HCO_3 solution (2.2% vol/vol of extraction buffer). All samples were then vortexed again for 10 seconds, incubated at −80 °C for 1–1.5 hours, thawed on ice and then centrifuged at 4 °C, 16,000*g* for 10 minutes. Supernatant was transferred to liquid chromatography–mass spectrometry (LC–MS) vials for analysis. The acid and associated neutralization are important for NAD(P)(H) measurement and were omitted for ^{13}C-labelled samples where NAD(P)(H) measurement was not the focus.

Saponified-fatty-acid extraction of tissue was done by adding 1 ml of 0.3 M KOH in 90:10 methanol/H_2O to the weighed tissue powder. After transferring the resulting mixture to a 4 ml glass vial, saponification was done at 80 °C in water bath for 1 hour. Then samples were cooled to room temperature, neutralized with 100 µl pure formic acid and extracted with 1 ml of hexane. The hexane layer was transferred to another glass vial, dried down under N_2, and resuspended in 1:1 methanol: acetonitrile (100 µl per mg tissue; 40 µl per µl serum) for LC–MS analysis.

Serum samples were collected by centrifuging blood at 16,000*g* at 4 °C for 10 minutes. Then serum was extracted as above for both water-soluble metabolites (final volume: 30 µl methanol per µl serum) and saponified fatty acids (final volume: 40 µl 1:1 methanol:acetonitrile per µl serum).

Acetate labelling in serum was measured with a derivatization method: 5 µl serum was added into 100 µl of a mixture of 12 mM 1-ethyl-3-(3-dimethylaminoproryl)carbodiimide (EDC), 15 mM 3-nitrophenylhydrazine, and pyridine (2% vol/vol) in methanol, incubated at 4 °C for 1 hour, and centrifuged for 10 minutes at 16,000*g*. Then the supernatant was quenched with 0.5 mM 2-mercaptoethanol and 0.1% formic acid in water and directly analysed by LC–MS[83].

Folate species were also measured by a derivatization method[84]. First, 20 mg of tissue was extracted with 1 ml of 1:1 methanol:H_2O with sodium ascorbate (25 mM) and ammonium acetate (25 mM). Precipitates were pelleted by centrifugation (16,000*g*, 10 minutes). The supernatants were dried down under N_2 and resuspended in 450 µl of H_2O with ascorbic acid (30 mM), dipotassium phosphate

(50 mM) and 2-mercaptoethanol (0.5%). Then 25 µl of charcoal-treated rat serum was added to each sample, and the resulting sample was incubated at 37 °C for 2 hours. Samples were cleaned by Bond Elut PH columns (Agilent Technologies). Columns were washed with 1 ml methanol and conditioned with 1 ml ascorbic acid buffer (30 mM ascorbic acid, 25 mM ammonium acetate in water). Samples were adjusted to pH 4 using formic acid and were loaded onto the columns. Each column was then washed with 1 ml of the ascorbic acid buffer. Folate species were eluted with 400 µl of 1:1 methanol:H_2O with 2-mercaptoethanol (0.5% vol/vol) and ammonium acetate (25 mM). The eluate was dried down under N_2, resuspended in HPLC H_2O, centrifuged (16,000*g*, 5 minutes) and analysed by LC–MS.

Serum triglycerides were extracted with ethyl acetate. Serum (4 µl) was added to ethyl acetate (100 µl) and centrifuged for 10 minutes at 16,000*g*, and the supernatant was collected. The extraction above was repeated once and supernatants combined. The resulting ethyl acetate extract was dried down and redissolved in 1:1:1 methanol:acetonitrile:2-propanol (200 µl) before analysis by LC–MS. Tissue triglycerides were extracted with 2-propanol. Tissue powder after grinding (5 mg) was added to 2-propanol (200 µl), vortexed for 10 seconds and then put on dry ice for 10 minutes. Samples were then centrifuged for 30 minutes at 16,000*g*, and the supernatant was used for LC–MS analysis.

LC–MS methods. LC–MS analysis for soluble metabolites was achieved on the Q Exactive PLUS hybrid quadrupole-orbitrap mass spectrometer (Thermo Scientific) coupled with hydrophilic interaction chromatography (HILIC)[24]. To perform the LC separation of ^{13}C-labelled tissue samples, cultured cell samples and all serum samples, an XBridge BEH Amide column (150 mm × 2.1 mm, 2.5 µM particle size, Waters) was used with a gradient of solvent A (95%:5% H_2O: acetonitrile with 20 mM ammonium acetate, 20 mM ammonium hydroxide, pH 9.4), and solvent B (100% acetonitrile). The gradient was 0 minutes, 85% B; 2 minutes, 85% B; 3 minutes, 80% B; 5 minutes, 80% B; 6 minutes, 75% B; 7 minutes, 75% B; 8 minutes, 70% B; 9 minutes, 70% B; 10 minutes, 50% B; 12 minutes, 50% B; 13 minutes, 25% B; 16 minutes, 25% B; 18 minutes, 0% B; 23 minutes, 0% B; 24 minutes, 85% B; 30 minutes, 85% B. The flow rate was 150 µl min^{-1}; the injection volume was 10 µl; the column temperature was 25 °C. MS full scans were in negative ion mode with a resolution of 140,000 at *m/z* 200 and scan range of 75–1,000 *m/z*. The automatic gain control (AGC) target was 1×10^6.

Deuterium-labelled tissue samples and cultured cell samples were analysed by an almost identical method with a modified gradient and a targeted NADP(H) scan. The gradient was: 0 minutes, 85% B; 2 minutes, 85% B; 3 minutes, 60% B; 9 minutes, 60% B; 9.5 minutes, 35% B; 13 minutes, 5% B; 15.5 minutes, 5% B; 16 minutes, 85% B, 20 minutes stop run, and the injection volume was 15 µl. Full scans as above were alternated with targeted scans: *m/z* 640–765 with a resolution of 35,000 at *m/z* = 200 (AGC target, 5×10^5).

To analyse serum acetate, we also used the Q Exactive PLUS hybrid quadrupole-orbitrap mass spectrometer. LC separation was on a reversed-phase column (Acquity UPLC BEH C18 column, 2.1 mm × 100 mm, 1.7 5 µm particle size, 130 Å pore size; Waters) using a gradient of solvent A (water), solvent B (methanol): 0 minutes, 10% B; 1 minute, 10% B; 5 minutes, 30% B; 11 minutes, 100% B; 14 minutes, 100% B; 14.5 minutes, 10% B; 22 minutes, 10% B. The flow rate was 200 µl min^{-1} and column temperature was 60 °C with an injection volume of 10 µl[83]. MS scans were in negative-ion mode with a resolution of 15,000 at *m/z* 200 and scan range of 100–300 *m/z*. The AGC target was 1×10^6.

To analyse folates[84], we again used the Q Exactive PLUS hybrid quadrupole-orbitrap mass spectrometer. LC separation was on a different reversed-phase column (Agilent InfinityLab Poroshell 120 Bonus-RP 2.7 µm, 2.1 × 150 mm) with a gradient of solvent A (1% vol of 1 M ammonium acetate and 0.1% vol of glacial acetic acid), solvent B (acetonitrile): 4 minutes, 80% B; 10 minutes, 2% B; 6 minutes, 30% B; 11 minutes, 100% B; 15 min, 100% B; 16 minutes, 2% B; 20 minutes 2% B. The flow rate was 200 µl min^{-1} and the column temperature was 25 °C with an injection volume of 20 µl. MS scans were in negative-ion mode with a resolution of 35,000 at *m/z* 200 and scan range of 350–1,000 *m/z*. The AGC target was 1×10^6.

To analyse fatty acids, we used an Exactive orbitrap mass spectrometer. LC separation was via reversed-phase ion-pairing chromatography on a Luna C8 column (150 × 2.0 mm^2, 3 µM particle size, 100 Å pore size; Phenomenex) with a gradient of solvent A (10 mM tributylamine + 15 mM acetic acid in 97:3 H_2O:methanol, pH 4.5), solvent B (methanol): 0 minutes 80% B; 10 minutes, 90% B; 11 minutes, 99% B; 25 minutes, 99% B; 26 minutes, 80% B; 30 minutes, 80% B. The flow rate was 250 µl min^{-1} and column temperature 25 °C with an injection volume of 5 µl. The MS scans were in negative-ion mode with a resolution of 100,000 at *m/z* 200 and scan range of 120–600. The AGC target was at high dynamic range.

To analyse triglycerides, we used a Q Exactive Plus mass spectrometer coupled to a Vanquish UHPLC system (Thermo Fisher Scientific) using positive-mode electrospray ionization. The LC separation was achieved on an Agilent Poroshell 120 EC-C18 column (150 × 2.1 mm, 2.7 µm particle size) at a flow rate of 150 µl min^{-1}. The gradient was 0 minutes, 25% B; 2 minutes, 25% B; 4 minutes, 65% B; 16 minutes, 100% B; 20 minutes, 100% B; 21 minutes, 25% B; 27 minutes, 25% B. Solvent A is 1 mM ammonium acetate + 0.2% acetic acid in water:methanol (90:10). Solvent B is 1 mM ammonium acetate + 0.2% acetic acid in methanol:2-propanol (2:98).

All data from labellling experiments were analysed by El-MAVEN[85] and subjected to natural abundance correction[86].

GC–MS for plasma D_2O measurement. Plasma D_2O was measured by headspace gas chromatography–mass spectrometry (GC–MS)[87]. First, 10 µl of plasma or D_2O standard sample was mixed with 5 µl 10 N sodium hydroxide and 10 µl acetone in a sealed 20 ml screw-top GC headspace vial (Agilent 5188-2573) at room temperature and the base-catalysed hydrogen (deuterium) exchange reaction between water/plasma water and acetone was allowed to proceed for 6 hours. D_2O standard samples were prepared by a serial two-third dilution of a solution of 30% D_2O down to 0.0135% D_2O in water. Then, 25 µl of each sample from headspace vial was injected into an Agilent GC–MS system (Agilent 7000D MS coupled with 7890B GC system) with a 2-minute isothermal run using a J&W HP-5ms GC column (Agilent 19091s-433, 30 m, 0.25 mm, 0.25 m) in split mode (10:1 split ratio). GC–MS parameters were: oven temperature 170 °C, inlet temperature 250 °C, source temperature 270 °C, MS1 quad temperature 150 °C, Aux-2 temperature 250 °C, He carrier flow 1 ml min^{-1}. Selected-ion monitoring was carried out for *m/z* 58–62. The ratio of integrated area of *m/z* 60 versus 59 from deuterated/unlabelled acetone (eluting at ~1.4 min) was determined.

Data analysis. Quantification of de novo lipogenesis flux with D_2O. Long-term steady-state analysis with oral D_2O. D_2O labels lipogenic fat both directly and via NADPH. Accordingly, a double binomial distribution model was used to calculate the palmitate labelling pattern on the basis of experimentally measured D_2O and NADPH labelling[24]. Fractional D_2O enrichment in vivo (p_1) was determined on the basis of labelling of soluble metabolites pairs (malate–fumarate; glutamate–α-ketoglutarate). NADPH active-H labelling (p_2) was calculated on the basis of the NADPH–NADP$^+$ pair (Supplementary Fig. 1):

$$\begin{bmatrix} M+0 & 0 \\ M+1 & M+0 \\ \vdots & M+1 \\ M+i & \vdots \\ 0 & M+i \end{bmatrix} \times \begin{bmatrix} 1-p \\ p \end{bmatrix} = \begin{bmatrix} M+0 \\ M+1 \\ \vdots \\ M+i \\ M+i+1 \end{bmatrix} \quad (1)$$

In the above equation, the matrix on the left-hand side contains the experimentally measured mass isotope distribution for the compound on the left-hand side in the equations in the schematic (Supplementary Fig. 1) (the same compound's mass isotope distribution is in both columns, offset as indicated). The matrix on the right-hand side contains the experimentally measured mass isotope distribution for the compound on the right-hand side in the above equations. The value of p is determined by solving the resulting linear equations. Values of $\boldsymbol{p}_1$ are the average of p determined using fumarate–malate and α-ketoglutarate–glutamate; p_2 is solely determined by NADP–NADPH. This method gives the same serum D_2O enrichment as standard GC–MS measurements (Extended Data Fig. 1f).

For the infusion of other deuterium tracers ([1-^{2}H]glucose and [2,3,3-^{2}H]-serine), NADPH active-H labelling was also calculated using equation (1).

Synthesis of one palmitate molecule (C16:0) requires 7 repeated reactions that incorporate 7 hydrogens from water and 14 hydrogens from NADPH. The expected (E) number of deuterium in one palmitate is:

$$E = 7 \times p_1 + 14 \times p_2 \quad (2)$$

Let M_i be the fraction of palmitate containing $\boldsymbol{i}$ deuterium atoms (that is, measured fraction at mass $M + i$ after correcting for natural isotope abundance). Then D is the average measured number of deuterium atoms accumulated at steady state per palmitate:

$$D = \sum_{i=0} M_i \times i \quad (3)$$

Where F is the de novo lipogenic fatty acid (palmitate) amount at steady state, C is the total fatty acid (palmitate) amount, and F/C is the fraction of palmitate synthesized de novo.

The total deuterium assimilated is given by both (1) the total fatty acid amount (C) times the measured average deuterium per fatty acid (D) and (2) the newly synthesized fatty acid amount (to be determined) times the expected deuterium per newly synthesized fatty acid (E):

$$C \times D = F \times E$$

$$\text{Fractional newly synthesized fatty acid at steady state} = \frac{F}{C} = \frac{D}{E} \quad (4)$$

Kinetic analysis of de novo lipogenesis with D_2O infusion. For the 12-hour infusion experiments, D_2O in serum is not at steady state and accordingly a slightly more complex calculation is required. D_2O increases linearly with infusion time (Supplementary Figure 1g). The final serum D_2O enrichment (p_1) can thus be written as a linear function of time (t) and the water labelling rate (k_1):

$$p_1 = t \times k_1 \tag{5}$$

Owing to the rapid H–D exchange flux, tissue NADPH labelling reaches equilibrium with serum water labelling quickly, and therefore tissue NADPH will also rise linearly over time (t) and the NADPH labelling rate (k_2):

$$p_2 = t \times k_2 \tag{6}$$

where:

$$k_2/k_1 = \mathrm{H}_{\mathrm{exchange}} \tag{7}$$

The expected deuterium per palmitate (E) will be:

$$E = 7 \times p_1 + 14 \times p_2 = 7 \times k_1 \times t + 14 \times k_2 \times t \tag{8}$$

Define f (g h^{-1}) as the average de novo lipogenesis flux of palmitate per hour. For an infusion of duration t hours, the total deuterium amount incorporated into newly synthesized palmitate is:

$$\int f \times E \, \mathrm{d}t = D \times C \tag{9}$$

$$f \times \left(\frac{7}{2} k_1 \times t^2 + 7 k_2 \times t^2\right) = D \times C \tag{10}$$

$$\frac{f}{C} = \frac{D}{(3.5k_1 + 7k_2) \times t^2} \tag{11}$$

Newly synthesized palmitate (F) in $t = 12$ hours is given by:

$$\frac{F}{C} = \frac{12 \times f}{C} = \frac{D}{(3.5k_1 + 7k_2) \times 12} \tag{12}$$

Quantification of direct carbon contribution from circulating substrates. The direct carbon sources for lipogenesis can be analysed similarly to the direct circulating nutrient contribution to TCA[26]. Because F_{circ} (ref. [26]) (the whole-body production rate of a metabolite) values for glucose, lactate and acetate are high, their labelling in serum reaches steady state within ~1 hour of infusion. Saponified fatty-acid labelling, however, does not reach steady state over 12 hours. So, an extra factor of newly synthesized fat ($\frac{F}{C}$ from equation (12)) needs to be included.

Here, we define $f_{\mathrm{Pal}\leftarrow\mathrm{Met}}$ as the carbon flux directly coming from a given circulating metabolite to palmitate. By direct, we mean that the circulating metabolite is taken up into the lipogenic tissue (liver or adipose) and converted within the tissue to acetyl-CoA that is used for fat synthesis. This contrasts with circulating metabolites that are converted into a different circulating lipogenic precursor before entering the lipogenic tissue to support fat synthesis. Here, we assessed six potential lipogenic substrates: glucose (glc), lactate (lac), acetate (act), glutamine (gln), alanine (ala) and citrate (cit).

$L_{\mathrm{Met2}\leftarrow\mathrm{Met1}}$ is the average pseudo-steady-state ^{13}C-labelled fraction per carbon in metabolite_2 after infusion of U-^{13}C-labelled metabolite_1 as the tracer. To calculate enrichment, let N_i be the fraction of the metabolite containing i ^{13}C atoms (after natural isotope correction), and n the total carbon number of the metabolite:

$$L_{\mathrm{Met}} = \frac{\sum_{i=0}^{n} N_i \times \mathrm{i}}{n} \tag{13}$$

$$L_{\mathrm{Met2}\leftarrow\mathrm{Met1}} = \frac{L_{\mathrm{Met2}}}{L_{\mathrm{Met1}}} \tag{14}$$

Define the pre-steady-state ^{13}C labelling measured in saponified palmitate as $L_{\mathrm{pal}\leftarrow\mathrm{Met1\_12h}}$. The expected pseudo-steady-state palmitate labelling is then given by dividing by the fraction of newly synthesized palmitate over the 12 hours:

$$L_{\mathrm{pal}\leftarrow\mathrm{Met1}} = \frac{L_{\mathrm{pal}\leftarrow\mathrm{Met1\_12h}}}{F/C} \tag{15}$$

Liver is fed by 22% systemic arterial blood and 78% portal vein blood[88]; brown adipose tissue is fed by arterial blood[83]. Artery labelling was calculated on the basis of tail vein blood labelling[26], and portal vein labelling was directly measured.

We can then solve the direct carbon flux to de novo lipogenesis in liver and brown adipose tissue with the following equation:

$$\begin{bmatrix} 1 & L_{\mathrm{lac}\leftarrow\mathrm{glc}} & L_{\mathrm{act}\leftarrow\mathrm{glc}} & L_{\mathrm{gln}\leftarrow\mathrm{glc}} & L_{\mathrm{ala}\leftarrow\mathrm{glc}} & L_{\mathrm{cit}\leftarrow\mathrm{glc}} \\ L_{\mathrm{glc}\leftarrow\mathrm{lac}} & 1 & L_{\mathrm{act}\leftarrow\mathrm{lac}} & L_{\mathrm{gln}\leftarrow\mathrm{lac}} & L_{\mathrm{ala}\leftarrow\mathrm{lac}} & L_{\mathrm{cit}\leftarrow\mathrm{lac}} \\ L_{\mathrm{glc}\leftarrow\mathrm{act}} & L_{\mathrm{lac}\leftarrow\mathrm{act}} & 1 & L_{\mathrm{gln}\leftarrow\mathrm{act}} & L_{\mathrm{ala}\leftarrow\mathrm{act}} & L_{\mathrm{cit}\leftarrow\mathrm{act}} \\ L_{\mathrm{glc}\leftarrow\mathrm{gln}} & L_{\mathrm{lac}\leftarrow\mathrm{gln}} & L_{\mathrm{act}\leftarrow\mathrm{gln}} & 1 & L_{\mathrm{ala}\leftarrow\mathrm{gln}} & L_{\mathrm{cit}\leftarrow\mathrm{gln}} \\ L_{\mathrm{glc}\leftarrow\mathrm{ala}} & L_{\mathrm{lac}\leftarrow\mathrm{ala}} & L_{\mathrm{act}\leftarrow\mathrm{ala}} & L_{\mathrm{gln}\leftarrow\mathrm{ala}} & 1 & L_{\mathrm{cit}\leftarrow\mathrm{ala}} \\ L_{\mathrm{glc}\leftarrow\mathrm{cit}} & L_{\mathrm{lac}\leftarrow\mathrm{cit}} & L_{\mathrm{act}\leftarrow\mathrm{cit}} & L_{\mathrm{gln}\leftarrow\mathrm{cit}} & L_{\mathrm{ala}\leftarrow\mathrm{cit}} & 1 \end{bmatrix} \times \begin{bmatrix} f_{\mathrm{pal}\leftarrow\mathrm{glc}} \\ f_{\mathrm{pal}\leftarrow\mathrm{lac}} \\ f_{\mathrm{pal}\leftarrow\mathrm{act}} \\ f_{\mathrm{pal}\leftarrow\mathrm{gln}} \\ f_{\mathrm{pal}\leftarrow\mathrm{ala}} \\ f_{\mathrm{pal}\leftarrow\mathrm{cit}} \end{bmatrix} = \begin{bmatrix} L_{\mathrm{pal}\leftarrow\mathrm{glc}} \\ L_{\mathrm{pal}\leftarrow\mathrm{lac}} \\ L_{\mathrm{pal}\leftarrow\mathrm{act}} \\ L_{\mathrm{pal}\leftarrow\mathrm{gln}} \\ L_{\mathrm{pal}\leftarrow\mathrm{ala}} \\ L_{\mathrm{pal}\leftarrow\mathrm{cit}} \end{bmatrix} \tag{16}$$

Quantification of fractional NADPH contribution from different production pathways. Deuterium-labelled metabolite tracers label NADPH's active-H[24]. Active-H labelling in NADPH was determined from the isotopic pattern of NADPH relative to NADP$^+$ (equation (1)). The fraction of NADPH coming from different pathways was calculated as described previously[24]:

$$\text{Fractional NADPH contribution} = \frac{\text{Active-H labelling} \times (\text{number of NADPH made by pathway})}{\text{substrate labelling} \times \left(1 - \mathrm{H}_{\mathrm{exchange}}\right)} \tag{17}$$

The number of NADPH made by pathway is 2 for the oxidative PPP and 1 otherwise. $\mathrm{H}_{\mathrm{exchange}}$ refers to the fraction of NADPH undergoing H–D exchange with water. Experimental measurements of NADPH and fat labelling after D_2O infusion gave $\mathrm{H}_{\mathrm{exchange}}$ in liver and brown adipose (equation (7) and Extended Data Fig. 4f,g). Tissue glucose-6-phosphate labelling was used as substrate labelling for calculation of the oxPPP contribution; tissue serine $M+2$ and $M+3$ labelling (summed) was used as substrate labelling for calculation of the serine contribution. No correction was made for the deuterium kinetic isotope effect.

Statistics. All statistical analysis was done using the two-sided unpaired Mann–Whitney test. Data distribution was assumed to be normal, but this was not formally tested.

Reporting Summary. Further information on research design is available in the Nature Research Reporting Summary linked to this article.

Data availability

Raw data are provided in source data files. Source data are provided with this paper.

Code availability

El-MAVEN v.12 and natural abundance correction software accucor are available online on GitHub.

Received: 10 August 2021; Accepted: 30 September 2021;
Published online: 29 November 2021

References

1. Lehninger A. L., Nelson D. L. & Cox M. M. *Lehninger Principles of Biochemistry* 6th edn (W. H. Freeman, 2013).
2. Yu, Y., Clippinger, A. J. & Alwine, J. C. Viral effects on metabolism: changes in glucose and glutamine utilization during human cytomegalovirus infection. *Trends Microbiol.* **19**, 360–367 (2011).
3. Heaton, N. S. et al. Dengue virus nonstructural protein 3 redistributes fatty acid synthase to sites of viral replication and increases cellular fatty acid synthesis. *Proc. Natl Acad. Sci. USA* **107**, 17345–17350 (2010).
4. Singh, A. et al. De novo lipogenesis represents a therapeutic target in mutant Kras non-small cell lung cancer. *FASEB J.* **32**, 7018–7027 (2018).
5. Stoiber, K. et al. Targeting de novo lipogenesis as a novel approach in anti-cancer therapy. *Br. J. Cancer* **118**, 43–51 (2018).
6. Lambert, J. E., Ramos-Roman, M. A., Browning, J. D. & Parks, E. J. Increased de novo lipogenesis is a distinct characteristic of individuals with nonalcoholic fatty liver disease. *Gastroenterology* **146**, 726–735 (2014).
7. Bence, K. K. & Birnbaum, M. J. Metabolic drivers of non-alcoholic fatty liver disease. *Mol. Metab.* **50**, 101143 (2020).

8. Jang, C. et al. The small intestine shields the liver from fructose-induced steatosis. *Nat. Metab.* **2**, 586–593 (2020).
9. Goldberg, R. P. & Brunengraber, H. Contributions of cytosolic and mitochondrial acetyl-CoA syntheses to the activation of lipogenic acetate in rat liver. *Adv. Exp. Med Biol.* **132**, 413–418 (1980).
10. Hellerstein, M. K., Wu, K., Kaempfer, S., Kletke, C. & Shackleton, C. H. Sampling the lipogenic hepatic acetyl-CoA pool in vivo in the rat. Comparison of xenobiotic probe to values predicted from isotopomeric distribution in circulating lipids and measurement of lipogenesis and acetyl-CoA dilution. *J. Biol. Chem.* **266**, 10912–10919 (1991).
11. Chen, L. et al. NADPH production by the oxidative pentose-phosphate pathway supports folate metabolism. *Nat. Metab.* **1**, 404–415 (2019).
12. Ghergurovich, J. M. et al. Glucose-6-phosphate dehydrogenase is not essential for K-ras-driven tumor growth or metastasis. *Cancer Res.* **80**, 3820–3829 (2020).
13. Yoshida, A. Hemolytic anemia and G6PD deficiency. *Science* **179**, 532–537 (1973).
14. Fan, J. et al. Quantitative flux analysis reveals folate-dependent NADPH production. *Nature* **510**, 298–302 (2014).
15. Liu, L. et al. Malic enzyme tracers reveal hypoxia-induced switch in adipocyte NADPH pathway usage. *Nat. Chem. Biol.* **12**, 345–352 (2016).
16. Simopoulos, A. P. Essential fatty acids in health and chronic disease. *Am. J. Clin. Nutr.* **70**, 560S–569S (1999).
17. Kingsbury, K. J., Paul, S., Crossley, A. & Morgan, D. M. The fatty acid composition of human depot fat. *Biochem. J.* **78**, 541–550 (1961).
18. Wadke, M., Brunengraber, H., Lowenstein, J. M., Dolhun, J. J. & Arsenault, G. P. Fatty acid synthesis by liver perfused with deuterated and tritiated water. *Biochemistry* **12**, 2619–2624 (1973).
19. Jungas, R. Fatty acid synthesis in adipose tissue incubated in tritiated water. *Biochemistry* **7**, 3708-& (1968).
20. Seyama, Y. et al. Identification of sources of hydrogen-atoms in fatty-acids synthesized using deuterated water and stereospecifically deuterium labeled nadph by gas-chromatographic mass-spectrometric analysis. *Biomed. Mass Spectrom.* **5**, 357–361 (1978).
21. Diraison, F., Pachiaudi, C. & Beylot, M. In vivo measurement of plasma cholesterol and fatty acid synthesis with deuterated water: determination of the average number of deuterium atoms incorporated. *Metabolism* **45**, 817–821 (1996).
22. Hellerstein, M. K. et al. Measurement of de novo hepatic lipogenesis in humans using stable isotopes. *J. Clin. Invest.* **87**, 1841–1852 (1991).
23. McCabe, B. J. & Previs, S. F. Using isotope tracers to study metabolism: application in mouse models. *Metab. Eng.* **6**, 25–35 (2004).
24. Zhang, Z., Chen, L., Liu, L., Su, X. & Rabinowitz, J. D. Chemical basis for deuterium labeling of fat and NADPH. *J. Am. Chem. Soc.* **139**, 14368–14371 (2017).
25. Hellerstein, M. K. No common energy currency: de novo lipogenesis as the road less traveled. *Am. J. Clin. Nutr.* **74**, 707–708 (2001).
26. Hui, S. et al. Glucose feeds the TCA cycle via circulating lactate. *Nature* **551**, 115–118 (2017).
27. Sanchez-Gurmaches, J. et al. Brown fat AKT2 is a cold-induced kinase that stimulates ChREBP-mediated de novo lipogenesis to optimize fuel storage and thermogenesis. *Cell Metab.* **27**, 195–209.e6 (2018).
28. Vijayakumar, A. et al. Absence of carbohydrate response element binding protein in adipocytes causes systemic insulin resistance and impairs glucose transport. *Cell Rep.* **21**, 1021–1035 (2017).
29. Hui, S. et al. Quantitative fluxomics of circulating metabolites. *Cell Metab.* **32**, 676–688 (2020).
30. Faubert, B. et al. Lactate metabolism in human lung tumors. *Cell* **171**, 358–371 (2017).
31. Gladden, L. B. Lactate metabolism: a new paradigm for the third millennium. *J. Physiol.* **558**, 5–30 (2004).
32. Gladden, L. B. A lactatic perspective on metabolism. *Med Sci. Sports Exerc.* **40**, 477–485 (2008).
33. Mashimo, T. et al. Acetate is a bioenergetic substrate for human glioblastoma and brain metastases. *Cell* **159**, 1603–1614 (2014).
34. Schug, Z. T. et al. Acetyl-CoA synthetase 2 promotes acetate utilization and maintains cancer cell growth under metabolic stress. *Cancer Cell* **27**, 57–71 (2015).
35. Comerford, S. A. et al. Acetate dependence of tumors. *Cell* **159**, 1591–1602 (2014).
36. Huang, Z. et al. ACSS2 promotes systemic fat storage and utilization through selective regulation of genes involved in lipid metabolism. *Proc. Natl Acad. Sci. USA* **115**, E9499–E9506 (2018).
37. Zhao, S. et al. Dietary fructose feeds hepatic lipogenesis via microbiota-derived acetate. *Nature* **579**, 586–591 (2020).
38. Nelson, M. E. et al. Inhibition of hepatic lipogenesis enhances liver tumorigenesis by increasing antioxidant defence and promoting cell survival. *Nat. Commun.* **8**, 14689 (2017).
39. Tasdogan, A. et al. Metabolic heterogeneity confers differences in melanoma metastatic potential. *Nature* **577**, 115–120 (2020).
40. Uhlén, M. et al. Proteomics. Tissue-based map of the human proteome. *Science* **347**, 1260419 (2015).
41. Lewis, C. A. et al. Tracing compartmentalized NADPH metabolism in the cytosol and mitochondria of mammalian cells. *Mol. Cell* **55**, 253–263 (2014).
42. Ölander, M., Wiśniewski, J. R. & Artursson, P. Cell-type-resolved proteomic analysis of the human liver. *Liver Int.* **40**, 1770–1780 (2020).
43. Ding, C. et al. A cell-type-resolved liver proteome. *Mol. Cell Proteom.* **15**, 3190–3202 (2016).
44. Battistuzzi, G., D'Urso, M., Toniolo, D., Persico, G. M. & Luzzatto, L. Tissue-specific levels of human glucose-6-phosphate dehydrogenase correlate with methylation of specific sites at the 3′ end of the gene. *Proc. Natl Acad. Sci. USA* **82**, 1465–1469 (1985).
45. Hao, Q. et al. Transcriptome profiling of brown adipose tissue during cold exposure reveals extensive regulation of glucose metabolism. *Am. J. Physiol. Endocrinol. Metab.* **308**, E380–E392 (2015).
46. Karlsson, M. et al. A single-cell type transcriptomics map of human tissues. *Sci. Adv.* https://doi.org/10.1126/sciadv.abh2169 (2021).
47. Metallo, C. M. et al. Reductive glutamine metabolism by IDH1 mediates lipogenesis under hypoxia. *Nature* **481**, 380–384 (2011).
48. MacParland, S. A. et al. Single cell RNA sequencing of human liver reveals distinct intrahepatic macrophage populations. *Nat. Commun.* **9**, 4383 (2018).
49. Davidson, S. M. et al. Environment impacts the metabolic dependencies of ras-driven non-small cell lung cancer. *Cell Metab.* **23**, 517–528 (2016).
50. Piskounova, E. et al. Oxidative stress inhibits distant metastasis by human melanoma cells. *Nature* **527**, 186–191 (2015).
51. MacFarlane, A. J. et al. Cytoplasmic serine hydroxymethyltransferase regulates the metabolic partitioning of methylenetetrahydrofolate but is not essential in mice. *J. Biol. Chem.* **283**, 25846–25853 (2008).
52. Ducker, G. S. et al. Reversal of cytosolic one-carbon flux compensates for loss of the mitochondrial folate pathway. *Cell Metab.* **24**, 640–641 (2016).
53. Ducker, G. S. et al. Human SHMT inhibitors reveal defective glycine import as a targetable metabolic vulnerability of diffuse large B-cell lymphoma. *Proc. Natl Acad. Sci. USA* **114**, 11404–11409 (2017).
54. Beaudin, A. E. et al. Shmt1 and de novo thymidylate biosynthesis underlie folate-responsive neural tube defects in mice. *Am. J. Clin. Nutr.* **93**, 789–798 (2011).
55. Meiser, J. et al. Serine one-carbon catabolism with formate overflow. *Sci. Adv.* **2**, e1601273 (2016).
56. Zheng, Y. et al. Mitochondrial one-carbon pathway supports cytosolic folate integrity in cancer cells. *Cell* **175**, 1546–1560 (2018).
57. Appling, D. R. Compartmentation of folate-mediated one-carbon metabolism in eukaryotes. *FASEB J.* **5**, 2645–2651 (1991).
58. Barlowe, C. K. & Appling, D. R. In vitro evidence for the involvement of mitochondrial folate metabolism in the supply of cytoplasmic one-carbon units. *Biofactors* **1**, 171–176 (1988).
59. Softic, S. et al. Dietary sugars alter hepatic fatty acid oxidation via transcriptional and post-translational modifications of mitochondrial proteins. *Cell Metab.* **30**, 735–753.e4 (2019).
60. Alwahsh, S. M. & Gebhardt, R. Dietary fructose as a risk factor for non-alcoholic fatty liver disease (NAFLD). *Arch. Toxicol.* **91**, 1545–1563 (2017).
61. Hellerstein, M. K., Schwarz, J. M. & Neese, R. A. Regulation of hepatic de novo lipogenesis in humans. *Annu Rev. Nutr.* **16**, 523–557 (1996).
62. Cohen, P. et al. Role for stearoyl-CoA desaturase-1 in leptin-mediated weight loss. *Science* **297**, 240–243 (2002).
63. Ducker, G. S. & Rabinowitz, J. D. One-carbon metabolism in health and disease. *Cell Metab.* **25**, 27–42 (2017).
64. Mullarky, E. et al. Inhibition of 3-phosphoglycerate dehydrogenase (PHGDH) by indole amides abrogates de novo serine synthesis in cancer cells. *Bioorg. Med. Chem. Lett.* **29**, 2503–2510 (2019).
65. Pacold, M. E. et al. A PHGDH inhibitor reveals coordination of serine synthesis and one-carbon unit fate. *Nat. Chem. Biol.* **12**, 452–458 (2016).
66. Locasale, J. W. Serine, glycine and one-carbon units: cancer metabolism in full circle. *Nat. Rev. Cancer* **13**, 572–583 (2013).
67. Yang, M. & Vousden, K. H. Serine and one-carbon metabolism in cancer. *Nat. Rev. Cancer* **16**, 650–662 (2016).
68. Ye, J. et al. Serine catabolism regulates mitochondrial redox control during hypoxia. *Cancer Discov.* **4**, 1406–1417 (2014).
69. Fu, X. et al. Measurement of lipogenic flux by deuterium resolved mass spectrometry. *Nat. Commun.* **12**, 3756 (2021).
70. Wallace, M. & Metallo, C. M. Tracing insights into de novo lipogenesis in liver and adipose tissues. *Semin. Cell Dev. Biol.* **108**, 65–71 (2020).
71. Strawford, A., Antelo, F., Christiansen, M. & Hellerstein, M. K. Adipose tissue triglyceride turnover, de novo lipogenesis, and cell proliferation in humans measured with 2H2O. *Am. J. Physiol. Endocrinol. Metab.* **286**, E577–E588 (2004).

72. Shi, Y. et al. -Adrenergic receptor agonist induced hepatic steatosis in mice: modeling nonalcoholic fatty liver disease in hyperadrenergic states. *Am. J. Physiol. Endocrinol. Metab.* **321**, E90–E104 (2021).
73. Brunengraber, H., Kelleher, J. K. & Des Rosiers, C. Applications of mass isotopomer analysis to nutrition research. *Annu Rev. Nutr.* **17**, 559–596 (1997).
74. Laugero, K. D. & Moberg, G. P. Energetic response to repeated restraint stress in rapidly growing mice. *Am. J. Physiol. Endocrinol. Metab.* **279**, E33–E43 (2000).
75. Svensson, R. U. et al. Inhibition of acetyl-CoA carboxylase suppresses fatty acid synthesis and tumor growth of non-small-cell lung cancer in preclinical models. *Nat. Med.* **22**, 1108–1119 (2016).
76. Esler, W. P. & Bence, K. K. Metabolic targets in nonalcoholic fatty liver disease. *Cell Mol. Gastroenterol. Hepatol.* **8**, 247–267 (2019).
77. Kim, C. W. et al. Acetyl CoA carboxylase inhibition reduces hepatic steatosis but elevates plasma triglycerides in mice and humans: a bedside to bench investigation. *Cell Metab.* **26**, 576 (2017).
78. Goedeke, L. et al. Acetyl-CoA carboxylase inhibition reverses NAFLD and hepatic insulin resistance but promotes hypertriglyceridemia in rodents. *Hepatology* **68**, 2197–2211 (2018).
79. Chondronikola, M. et al. Brown adipose tissue improves whole-body glucose homeostasis and insulin sensitivity in humans. *Diabetes* **63**, 4089–4099 (2014).
80. Stanford, K. I. et al. Brown adipose tissue regulates glucose homeostasis and insulin sensitivity. *J. Clin. Invest.* **123**, 215–223 (2013).
81. Tuli, J. S., Smith, J. A. & Morton, D. B. Stress measurements in mice after transportation. *Lab Anim.* **29**, 132–138 (1995).
82. Rong, X. et al. LXRs regulate ER stress and inflammation through dynamic modulation of membrane phospholipid composition. *Cell Metab.* **18**, 685–697 (2013).
83. Jang, C. et al. Metabolite exchange between mammalian organs quantified in pigs. *Cell Metab.* **30**, 594–606 (2019).
84. Chen, L., Ducker, G. S., Lu, W., Teng, X. & Rabinowitz, J. D. An LC–MS chemical derivatization method for the measurement of five different one-carbon states of cellular tetrahydrofolate. *Anal. Bioanal. Chem.* **409**, 5955–5964 (2017).
85. Melamud, E., Vastag, L. & Rabinowitz, J. D. Metabolomic analysis and visualization engine for LC–MS data. *Anal. Chem.* **82**, 9818–9826 (2010).
86. Su, X., Lu, W. & Rabinowitz, J. D. Metabolite spectral accuracy on orbitraps. *Anal. Chem.* **89**, 5940–5948 (2017).
87. Shah, V., Herath, K., Previs, S. F., Hubbard, B. K. & Roddy, T. P. Headspace analyses of acetone: a rapid method for measuring the 2H-labeling of water. *Anal. Biochem.* **404**, 235–237 (2010).
88. Eipel, C., Abshagen, K. & Vollmar, B. Regulation of hepatic blood flow: the hepatic arterial buffer response revisited. *World J. Gastroenterol.* **16**, 6046–6057 (2010).

Acknowledgements

This work was supported by NIH Pioneer award 1DP1DK113643 and Pfizer. T.T. is supported by NIH fellowship 1F32DK118856. L.Y. was supported by a postdoctoral fellowship from the New Jersey Commission on Cancer Research. We thank X. Rong for input and advice. We thank S. Hui, C. Jang, L. Chen, Y. Shen, L. Wang, C. Bartman and all other Rabinowitz lab members for advice.

Author contributions

Z.Z., T.T. and J.D.R. came up with the general approach and experimental strategy. Z.Z. and T.T. designed and performed the in vivo and in vitro experiments and data interpretation. X.X. performed folate species measurement. X.Z. performed acetate measurement. L.Y. contributed to the initial discovery of serine-mediated NADPH production in liver. G.X., G.J.T. and M.F.C. contributed to in vitro tracing experiments and GC–MS analysis. Z.Z., T.T. and J.D.R. wrote the manuscript with help from all authors.

Competing interests

G.X., G.J.T. and M.F.C. are current employees of Pfizer and may be Pfizer shareholders. J.D.R. is a consultant and received research funding from Pfizer and is an adviser and stock owner in Colorado Research Partners, L.E.A.F. Pharmaceuticals, Rafael Pharmaceuticals, Barer Institute and its subsidiaries, Serien Therapeutics, Toran, Kadmon Pharmaceuticals and Agios Pharmaceuticals. J.D.R. is co-inventor of SHIN2 and related SHMT inhibitors, which have been patented by Princeton University. The remaining authors declare no competing interests.

Additional information

Extended data is available for this paper at https://doi.org/10.1038/s42255-021-00487-4.

Supplementary information The online version contains supplementary material available at https://doi.org/10.1038/s42255-021-00487-4.

Correspondence and requests for materials should be addressed to Joshua D. Rabinowitz.

Peer review information Primary Handling Editor: Christoph Schmitt

Reprints and permissions information is available at www.nature.com/reprints.

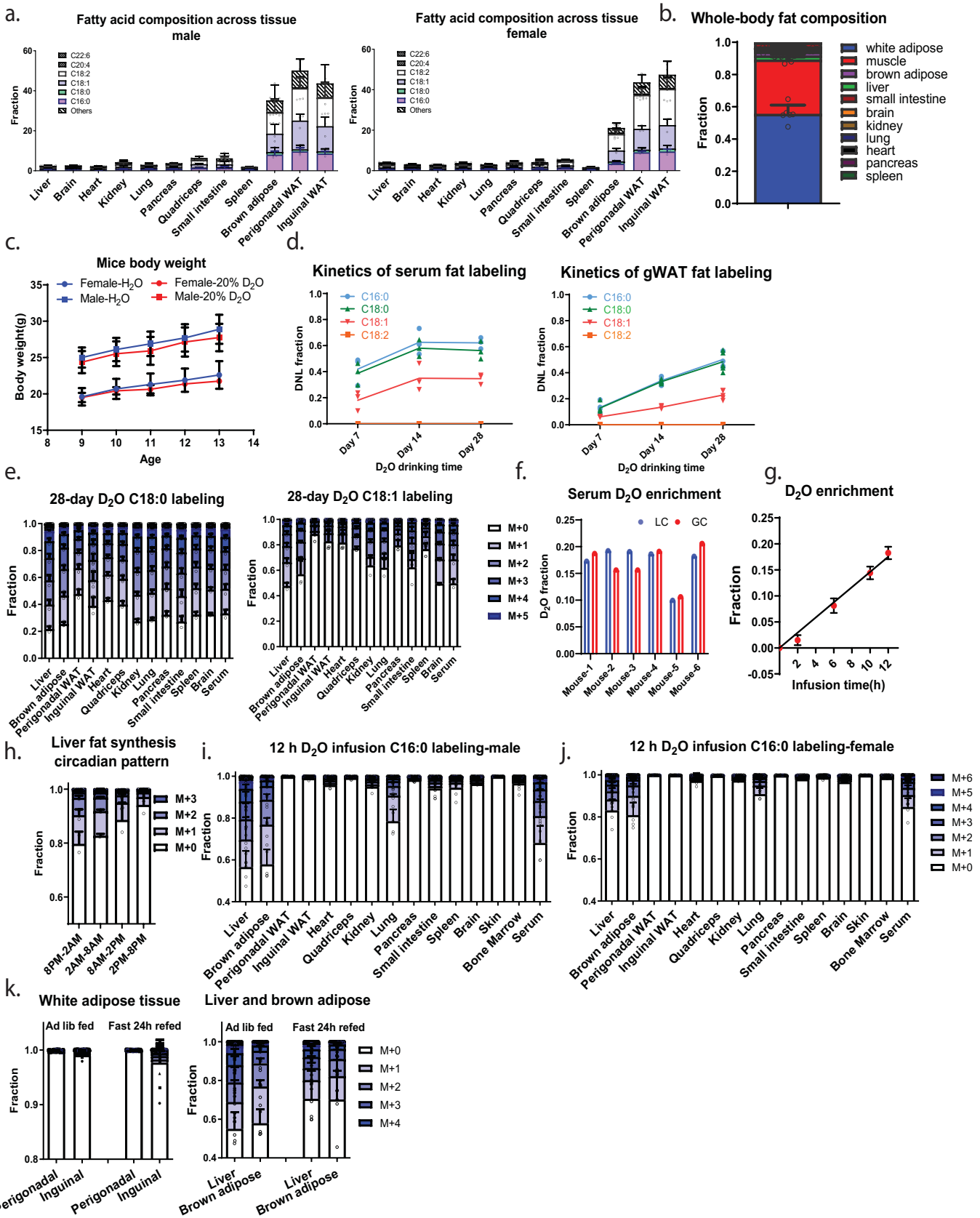

Extended Data Fig. 1 | See next page for caption.

Extended Data Fig. 1 | Fatty acid composition and D_2O labeling across tissues and time. (**a**) Fraction of tissue weight that is fat, and composition of those fatty acids in male and female mice. (**b**) Fat is stored in white adipose tissue, and to a lesser extent in muscle. Muscle values are calculated assuming quadriceps is representative of whole-body muscle. (**c**) Body weight of mice drinking 20% D_2O for 4 weeks (control data are from Jackson lab website). (**d**) Fatty acid labeling from D_2O reaches steady-state more quickly in serum than in white adipose, while different fatty acid species reach steady-state at a similar rate. (**e**) C18:0 and oleate (C18:1) labeling pattern across tissues after 4 weeks of D_2O drinking. (**f**) Serum D_2O enrichment measured by LC-MS and GC-MS. (**g**) Labeling of serum D_2O increases linearly over time for the 12 h of infusion. (**h**) Circadian pattern of liver fat synthesis based on 6 h D_2O infusions. (**i**) C16:0 labeling pattern across tissues after 12 h fed-state D_2O infusion in male mice. (**j**) As is (j), for female mice. (**k**) C16:0 labeling in white adipose tissue, liver, and brown adipose tissue from 12 h refed D_2O infusion after 24 h fast. Mean ± s.d., n = 3 of both genders for fat composition analysis; n = 4 male mice for steady-state analysis and body composition analysis; n = 4 of both genders for bodyweight measurement; n = 2 male mice for 6 h D_2O infusions; n = 5 of both genders for 12 h D_2O infusion; n = 5 males in each group for the fasted-refed experiments.

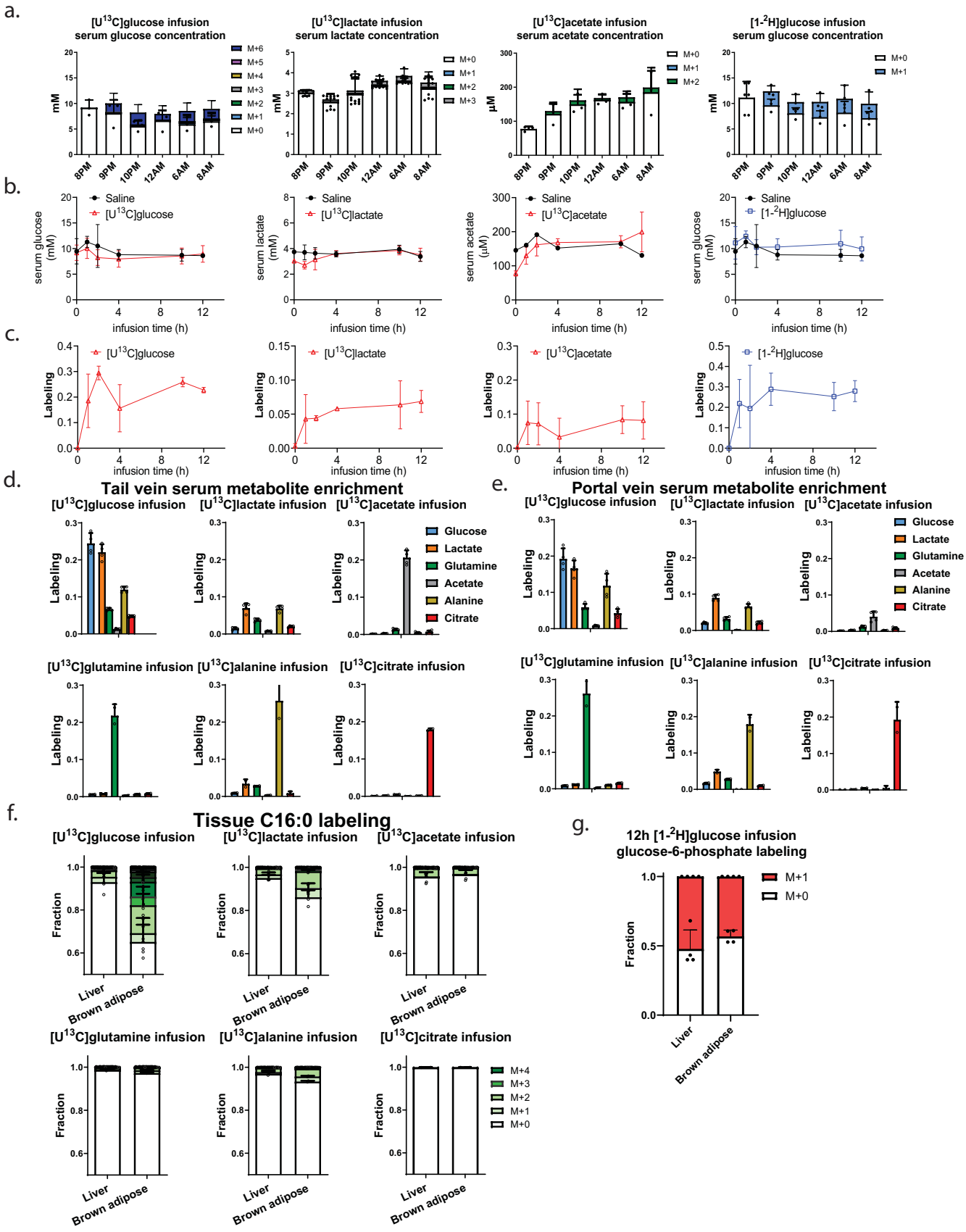

Extended Data Fig. 2 | See next page for caption.

Extended Data Fig. 2 | Circulating metabolite levels and labeling and tissue saponified fat labeling from carbon tracers and [1-^{2}H]glucose. (**a**) Circulating concentrations of unlabeled and labeled forms during the indicated tracer infusions. (**b**) Corresponding total concentrations. (**c**) Corresponding average carbon atom labeling (for the 13 C tracers) or labeled fraction (for the [1-^{2}H]glucose tracer). (**d**) Tail vein serum circulating metabolite average carbon atom labeling from different infused ^{13}C tracers (each sampled at end of 12 h infusion). (**e**) As in (d), from portal vein. (**f**) Corresponding C16:0 labeling in liver and brown adipose. (**g**) Glucose-6-phosphate labeling from 12 h [1-^{2}H]glucose infusion in liver and brown adipose tissue. All data are mean ± s.d. For time-point samples, [U-^{13}C]glucose (n = 3), lactate (n = 3), acetate (n = 3), [1-^{2}H]glucose (n = 4), saline (n = 2); for other samples [U-^{13}C]glucose (n = 4), lactate (n = 4), glutamine (n = 2), acetate (n = 4), alanine (n = 2) citrate (n = 2) and [1-^{2}H]glucose (n = 4). All mice are males. For female data, see Extended Data Fig. 6.

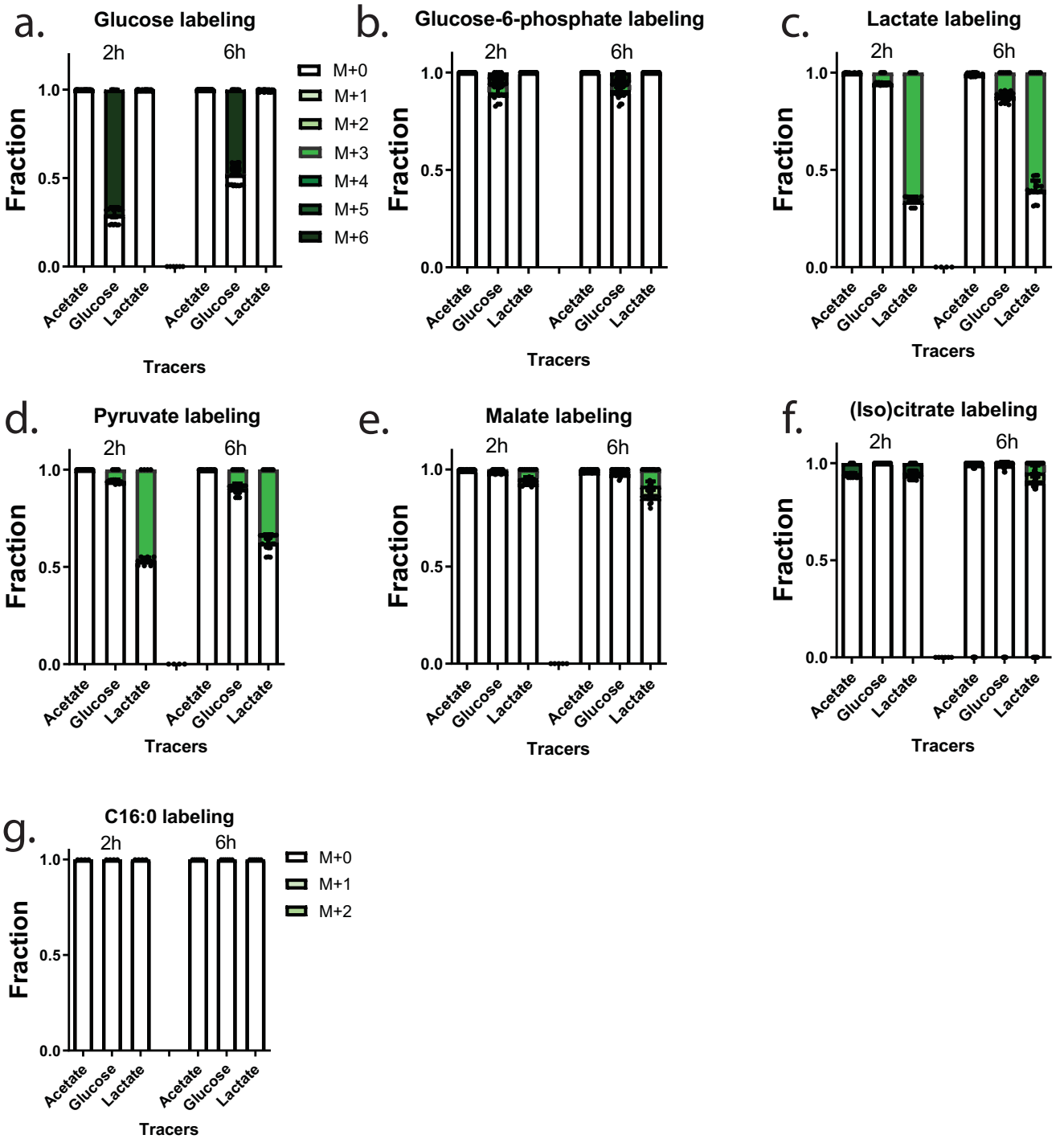

Extended Data Fig. 3 | Carbon tracing in liver slices. (a-g). Labeling of the indicated metabolites in liver slices after 2 h or 6 h incubation in Krebs-Ringer buffer containing glucose, lactate, and acetate, with the indicated metabolite provided in [U^{13}C]-labeled form. Data are mean ± s.d.; n = 2 mice for 2 h experiments; n = 3 mice for 6 h experiments, 2 technical replicates (independent tissue slices) from each mouse liver. All mice are males.

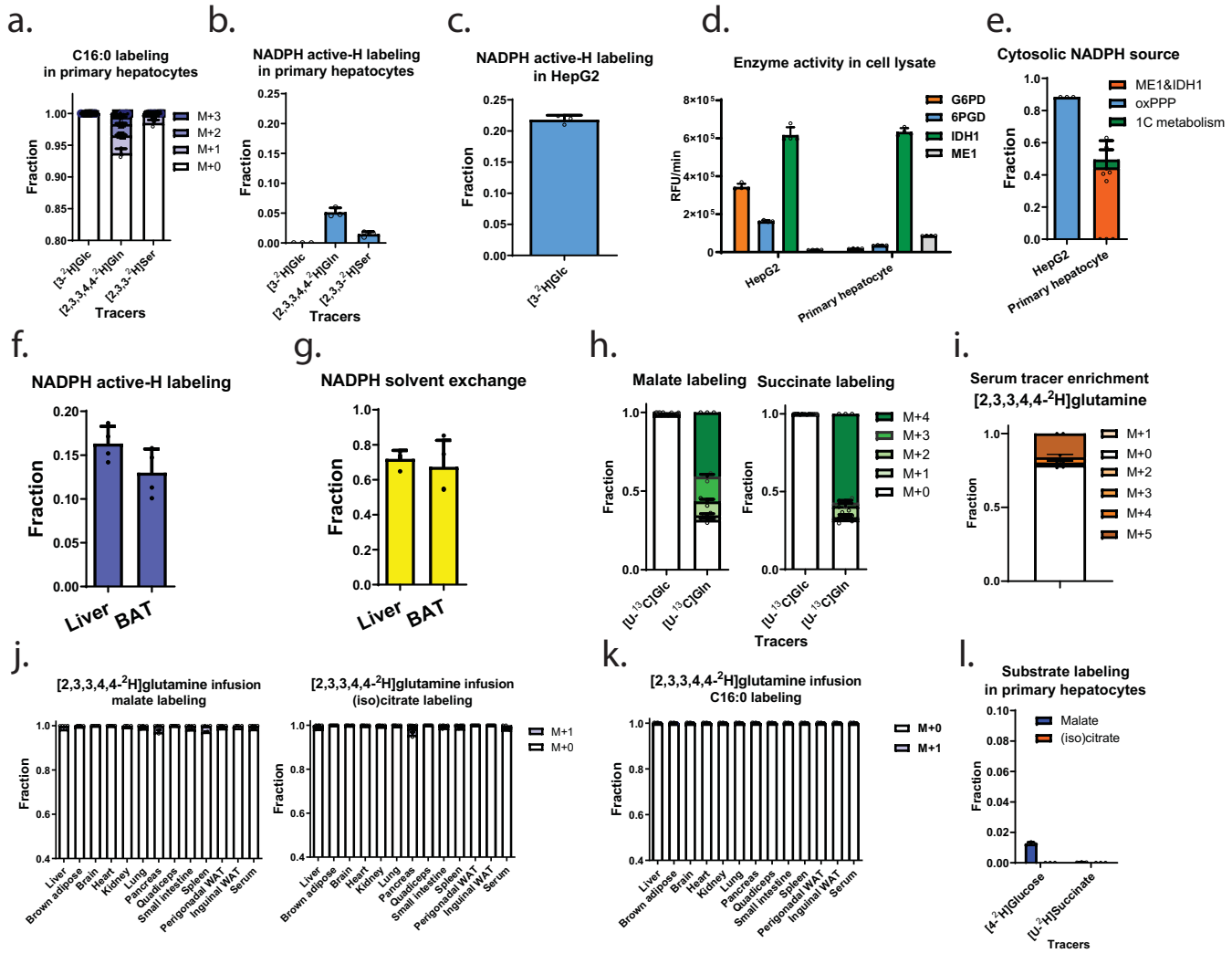

Extended Data Fig. 4 | Hepatocytes are deficient in the oxPPP, and [2,3,3,4,4-^{2}H]glutamine tracer works to probe malic enzyme and IDH flux in cultured hepatocytes but not *in vivo*. (**a**) C16:0 labeling over 6 h from different tracers in primary hepatocytes. (**b**) NADPH active-H labeling over 2.5 h from different tracers in primary hepatocytes. (**c**) NADPH active-H measurement over 2.5 h from [3-^{2}H]glucose in HepG2 cells. (**d**) Enzymatic activity of G6PD, 6PGD, IDH1 and ME1 in lysates from HepG2 cells and primary murine hepatocytes. (**e**) Hydride sources supporting *de novo* lipogenesis in HepG2 cells and primary hepatocytes, correcting for substrate labeling and H-D exchange between NADPH and water. (**f**) NADPH active hydrogen labeling from 12 h D_2O infusion in liver and brown adipose. (**g**) The fraction of active hydrogen on NADPH that undergoes solvent exchange with water calculated from 12 h D_2O infusion in liver and brown adipose. (**h**) Glutamine is the dominant TCA substrate in cultured primary hepatocytes. (**i**) Serum tracer labeling at the end of 12 h [2,3,3,4,4-^{2}H]glutamine infusion. (**j**) Minimal malate and (iso)citrate labeling from [2,3,3,4,4-^{2}H]glutamine infusion across tissues *in vivo*. (**k**) C16:0 labeling from [2,3,3,4,4-^{2}H]glutamine infusion across tissues. (**l**) Minimal malate and (iso)citrate labeling from [4-^{2}H]glucose and [U-^{2}H]succinate in cultured primary hepatocytes. All data are mean ± s.d., n = 4 for solvent exchange measurement, n = 2 for [2,3,3,4,4-^{2}H]glutamine infusion, all mice are males, n = 3 biological replicates for all cell culture experiments.

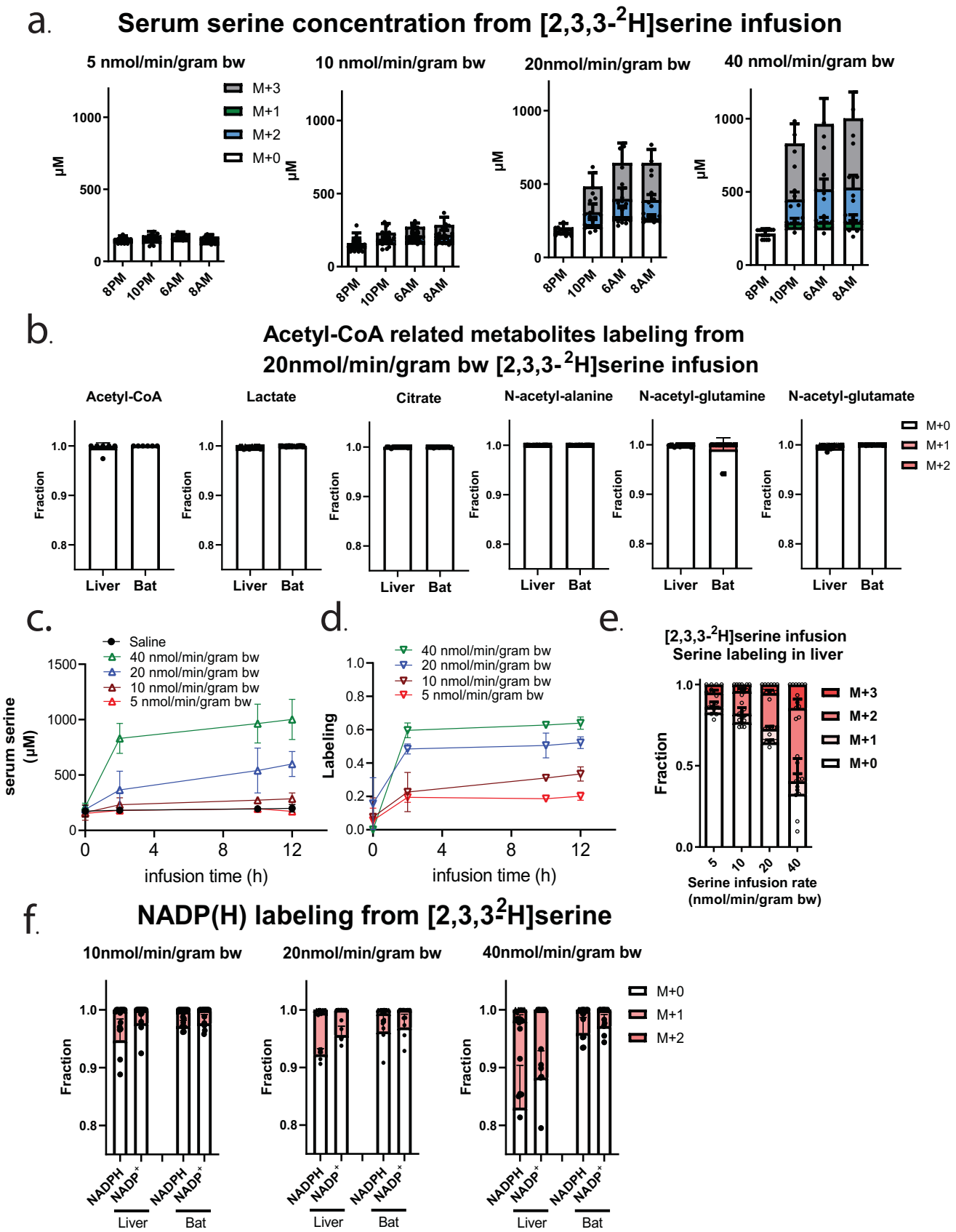

Extended Data Fig. 5 | See next page for caption.

Extended Data Fig. 5 | Serine's hydride contribution to liver fat across 8-fold range of [2,3,3-^{2}H]serine infusion rates. (**a**) Circulating serine labeling during [2,3,3-^{2}H]serine infusion at different rates, ranging from minimally to highly perturbative. (**b**) Lack of labeling in liver acetyl-CoA and related metabolites from 12 h [2,3,3-^{2}H]serine infusion (20 nmol/min/gram body weight). (**c**) Circulating serine concentrations during [2,3,3-^{2}H]serine infusion at different rates, ranging from minimally to highly perturbative (sum of unlabeled and labeled). (**d**) Corresponding serine labeling (average atom labeling of serine side chain hydrogens). (**e**) Liver serine labeling after 12 h [2,3,3-^{2}H]serine infusion. (**f**) Corresponding liver and brown adipose tissue NADP(H) labeling. All data are mean ± s.d., For time point experiments n = 3 for each tracer and n = 2 for saline. For C16:0, NADPH, acetyl-CoA, and related metabolite labeling, n = 4 for 5 nmol/min/gram bodyweight and n = 6 for 10, 20 and 40 nmol/min/gram bodyweight of [2,3,3-^{2}H]serine infusion. All mice are males.

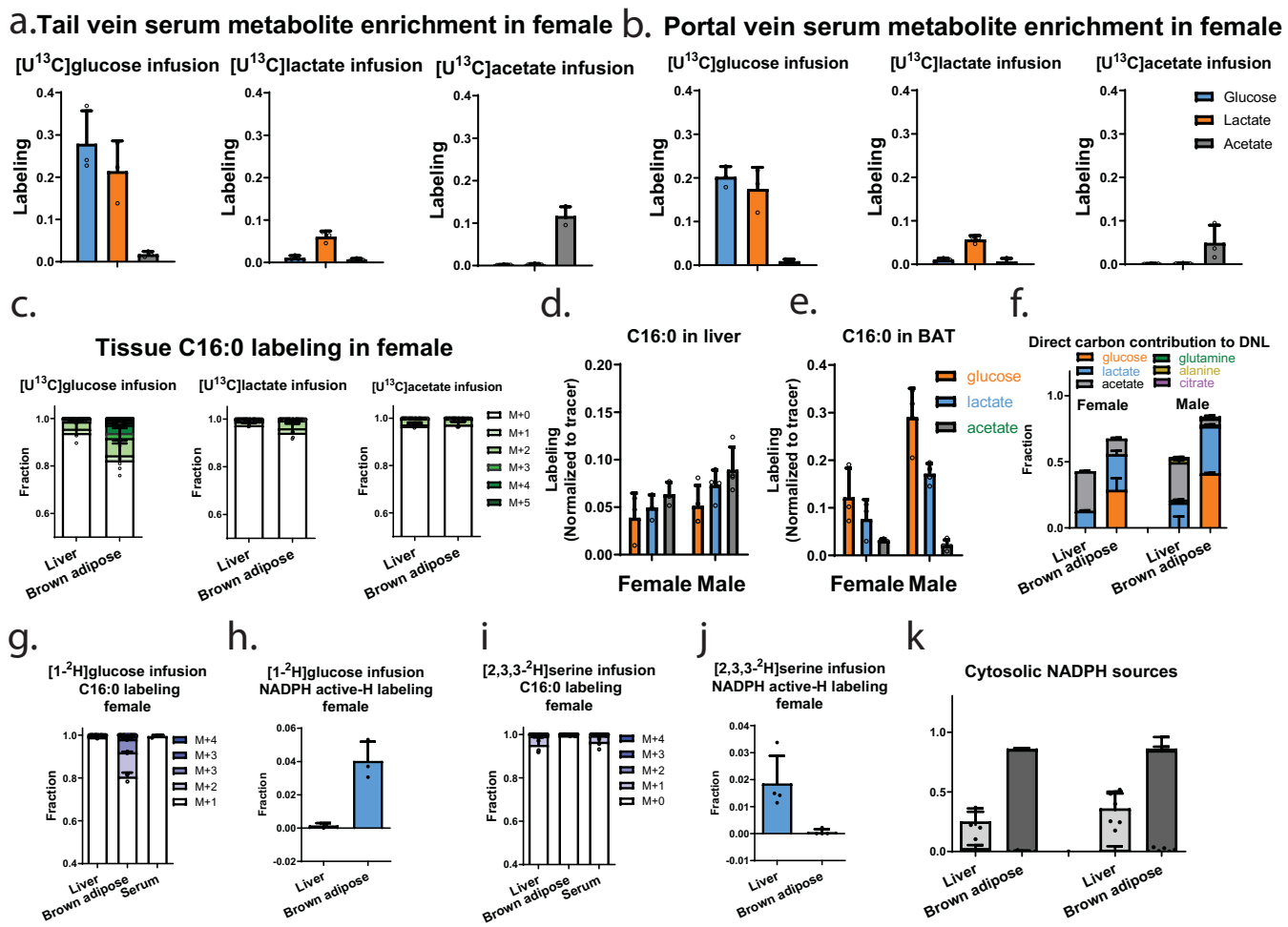

Extended Data Fig. 6 | Carbon and hydrogen inputs to lipogenesis are consistent across female and male mice. (**a**) Tail vein serum circulating metabolite average carbon atom labeling from different infused ^{13}C tracers (each after 12 h infusion) in female mice. (**b**) Corresponding portal vein serum circulating metabolite labeling in female mice. (**c**) Corresponding C16:0 labeling in liver and brown adipose in female mice. (**d**) Fractional enrichment of liver C16:0 in female mice following 12 h infusion of [U-^{13}C]-labeled glucose (n = 3), lactate (n = 3), acetate (n = 3). Male data are the same as Fig. 2a. Labeling is normalized to circulating tracer enrichment. Brown adipose is fueled by systemic blood (approximated by tail vein sampling) and liver is fueled by 78% portal vein blood and 22% systemic blood. (**e**) As is (d), for brown adipose C16:0. Male data are the same as in Fig. 2b. (**f**) Carbon sources supporting *de novo* lipogenesis in liver and brown adipose in female and male mice, based on direct contributions to C16:0, calculated based on data in (d) and (e). Male data are the same as Fig. 2d. (**g**) C16:0 labeling in liver, brown adipose and serum following 12 h [1-^{2}H]glucose infusion (125 nmol/min/gram body weight) in female mice (n = 3). (**h**) NADPH active-H measurement in liver and brown adipose from 12 h [1-^{2}H]glucose infusion (125 nmol/min/gram bw) in female mice (n = 4). (**i**) As is (g), for 12 h [2,3,3-^{2}H]serine infusion (20 nmol/min/gram bw). (**j**) As is (h), for 12 h [2,3,3-^{2}H]serine infusion (20 nmol/min/gram bw). (**k**) Hydride sources supporting *de novo* lipogenesis in liver and brown adipose in female (left-hand bars) and male (right-hand bars) mice, correcting for substrate labeling and H-D exchange between NADPH and water. Calculated based on tracer data in (h) and (j) and D_2O exchange data in Extended Data Fig. 4f. Male data are the same as in Fig. 4g. Light bars indicate contribution from 1C metabolism; dark bars indicate contribution from oxPPP. Data in f are mean ± s.e.m.; other data are mean ± s.d.

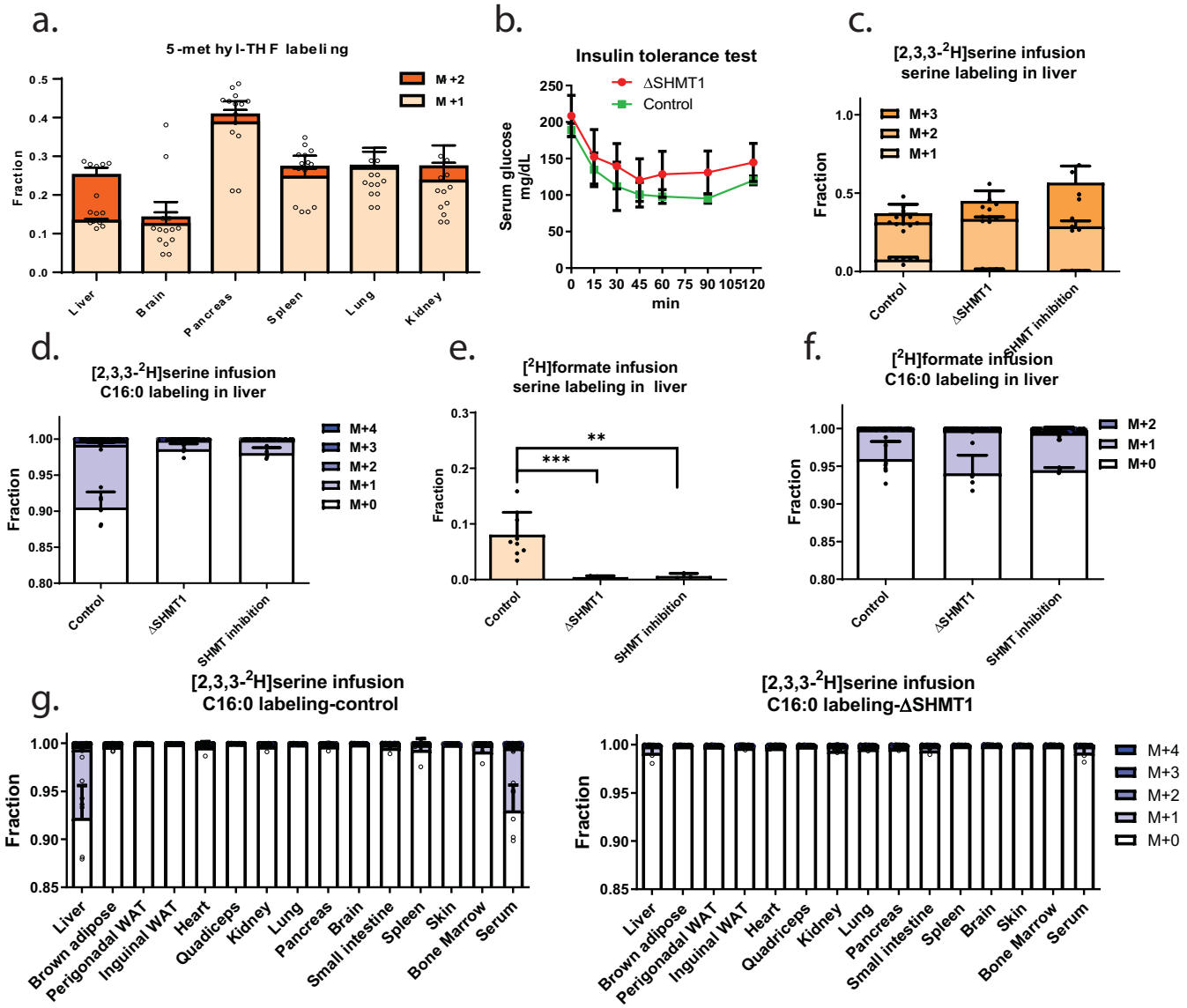

Extended Data Fig. 7 | Cytosolic serine catabolism in the liver is blunted by SHMT knockout or inhibition. (**a**) 5-methyl-THF labeling from 12 h [2,3,3-^{2}H]serine (20 nmol/min/gram body weight). M + 2 labeling reflects cytosolic serine catabolism. M + 1 labeling reflects the combination of mitochondrial serine catabolism and reversible flux through MTHFD1. (**b**) Glucose levels after insulin tolerance test in control and whole-body ΔSHMT1 mice. (**c**) Serine labeling in liver from 12 h [2,3,3-^{2}H]serine infusion (20 nmol/min/gram bw) in control, whole-body ΔSHMT1 mice, and mice treated with the dual SHMT1/2 inhibitor SHIN2 (3.33 mg/kg/h i.v. infusion). (**d**) C16:0 labeling in liver from 12 h [2,3,3-^{2}H]serine infusion (20 nmol/min/gram bw). (**e**) As is (c), for [^{2}H]formate infusion. (control vs. ΔSHMT1, p = 0.0010; control vs. SHIN2 treatment, p = 0.0091). (**f**) As is (d), for [^{2}H]formate infusion. (**g**) C16:0 labeling across tissues following 12 h [2,3,3-2H]serine infusion (20 nmol/min/gram body weight) in control and ΔSHMT1 mice. Mean ± s.d. For insulin tolerance tests, n = 12 for SHMT1 knock out mice, n = 4 for littermate wild type controls. For serine and formate infusions, n = 6 for control, n = 4 for ΔSHMT1, n = 4 for SHIN2 treatment. For [2,3,3-^{2}H]serine infusion in ΔSHMT1 mice, n = 4 for liver, bat, brain bone marrow, serum, and skin; n = 3 for other tissues; control mice data are the same as Fig. 4b. For D_2O tracing experiments, n = 10 in each group. *p < 0.05; **p < 0.01; ***p < 0.005 by unpaired Mann-Whitney test. All mice are males.

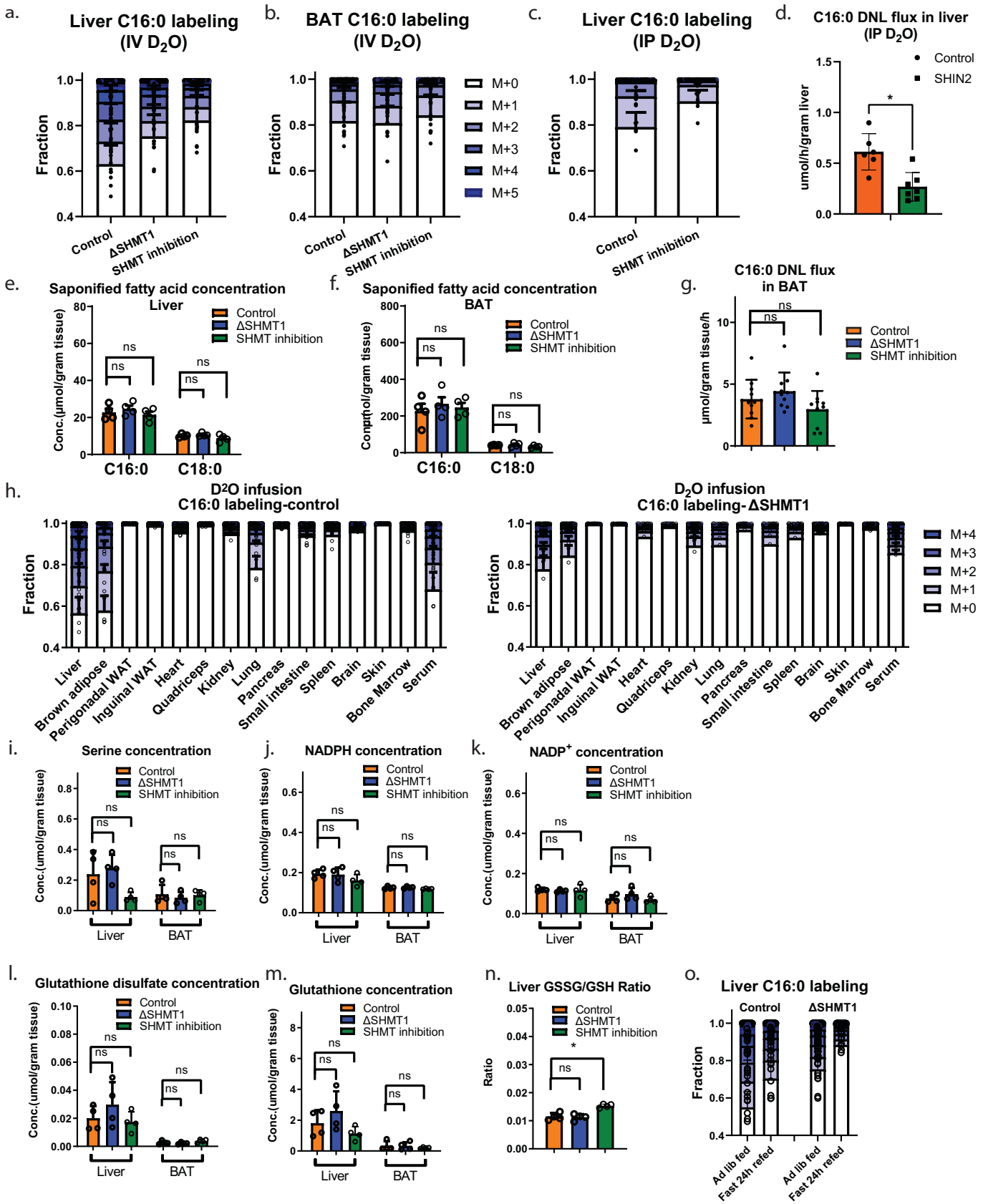

Extended Data Fig. 8 | See next page for caption.

Extended Data Fig. 8 | Concentrations and labeling of saponified fatty acids and soluble metabolites in wild type, ΔSHMT1, and SHMT inhibitor-treated mice (3.33 mg/kg/h i.v. infusion of SHIN2 for 12 h). (**a**) Saponified C16:0 labeling pattern in liver following 12 h D_2O infusion to control, ΔSHMT1, and SHIN2-treated mice (SHIN2 infused simultaneous with the D_2O infusion). (**b**) As is (a), for brown adipose. (**c**) Saponified C16:0 labeling pattern in liver following 12 h IP D_2O to control and SHIN2-treated mice (SHIN2 infused simultaneously). (**d**) C16:0 lipogenesis flux in liver overnight, as measured by IP D_2O injection. (control vs. SHIN2 treatment, $p = 0.0047$). (**e**) C16:0 and C18:0 concentration in liver of control, ΔSHMT1, and SHIN2-treated mice (control vs. ΔSHMT1, $p = 0.48$ for C16:0, $p = 0.88$ for C18:0; control vs. inhibitor, $p = 0.48$ for C16:0, $p = 0.34$ for C18:0). (**f**) As is (a), for brown adipose tissue (control vs. ΔSHMT1, $p = 0.68$ for C16:0, $p = 0.99$ for C18:0; control vs. SHIN2 treatment, $p = 0.99$ for C16:0, $p = 0.11$ for C18:1). (**g**) C16:0 lipogenesis flux in brown adipose tissue overnight, as measured by 12 h D_2O infusion (control vs. ΔSHMT1, $p = 0.32$; control vs. SHIN2 treatment, $p = 0.28$). (**h**) C16:0 labeling across tissues following 12 h D_2O infusion in control and ΔSHMT1 mice. (**i**) Serine concentration in liver and brown adipose tissue of control, ΔSHMT1, and SHIN2-treated mice (control vs. ΔSHMT1, $p = 0.99$ for liver, $p = 0.99$ for BAT; control vs. SHIN2 treatment, $p = 0.34$ for liver, $p = 0.34$ for BAT). (**j**) As is (i), for NADPH (control vs. ΔSHMT1, $p = 0.99$ for liver, $p = 0.88$ for BAT; control vs. SHIN2 treatment, $p = 0.11$ for liver, $p = 0.20$ for BAT). (**k**) As is (i), for $NADP^+$ (control vs. ΔSHMT1, $p = 0.34$ for liver, $p = 0.34$ for BAT; control vs. SHIN2 treatment, $p = 0.68$ for liver, $p = 0.48$ for BAT). (**l**) As is (i), for glutathione (control vs. ΔSHMT1, $p = 0.34$ for liver, $p = 0.68$ for BAT; control vs. SHIN2 treatment, $p = 0.48$ for liver, $p = 0.99$ for BAT). (**m**) As is (i), for glutathione disulfide (control vs. ΔSHMT1, $p = 0.34$ for liver, $p = 0.88$ for BAT; control vs. SHIN2 treatment, $p = 0.88$ for liver, $p = 0.14$ for BAT). (**n**) Liver glutathione disulfide vs. reduced glutathione ratio in control, ΔSHMT1, and SHIN2-treated mice (control vs. ΔSHMT1, $p = 0.99$; control vs. SHIN2 treatment, $p = 0.029$). (**o**) Liver C16:0 labeling pattern after 12 h D_2O infusion during ad lib feeding and in mice subjected to 24 h fasting followed by refeeding (control data are the same as Extended Data Fig. 1i; ΔSHMT1 ad lib fed data are the same as Extended Data Fig. 8h). Mean± s.d, $n = 4$ for control, ΔSHMT1, and SHIN2-treated mice. For refeeding experiment, $n = 3$ for ΔSHMT1 refed. For D_2O infusion in ΔSHMT1 mice, $n = 2$ for liver, bat, white adipose, lung, brain, bone marrow, serum, and skin; $n = 1$ for other tissues; control mice data are the same as Extended Data Fig. 1i. *$p < 0.05$ by unpaired Mann-Whitney test. All mice are males.

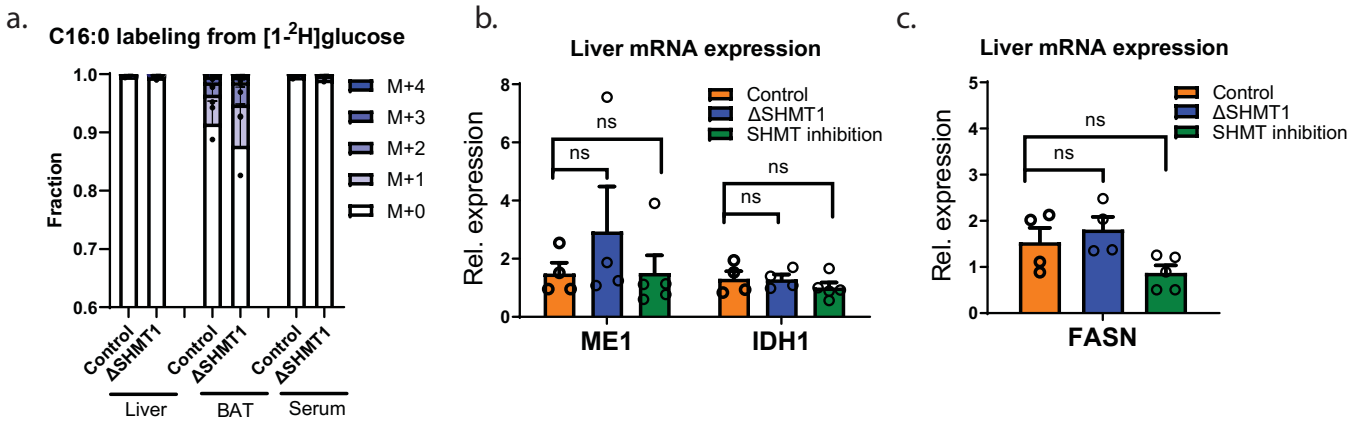

Extended Data Fig. 9 | Knockout of SHMT1 does not induce alternative NADPH producing enzymes. (**a**) C16:0 labeling from [1-^{2}H]glucose in liver, brown adipose tissue, and serum in control and ΔSHMT1 mice. (**b**) Relative mRNA expression level of Malic Enzyme 1 (ME1) and Isocitrate dehydrogenase 1 (IDH1) in liver of control, ΔSHMT1, and 12 h SHIN2 treated mice (3.33 mg/kg/h i.v. infusion) (control vs. ΔSHMT1, p = 0.48 for ME1, p = 0.88 for IDH1; control vs. inhibitor, p = 0.73 for ME1, p = 0.56 for IDH1.). (**c**) Relative mRNA expression level of fatty acid synthase (FASN) in liver of control, ΔSHMT1, and 12 h SHIN2 treated mice (3.33 mg/kg/h i.v. infusion) (control vs. ΔSHMT1, p = 0.48 for control vs. inhibitor, p = 0.26.) Mean± s.d. N = 2 mice in each group for [1-^{2}H]glucose infusion. For qPCR, n = 4 for control, n = 4 for ΔSHMT1, n = 5 for SHIN2 treatment, p-values from unpaired Mann-Whitney test. All mice are males.

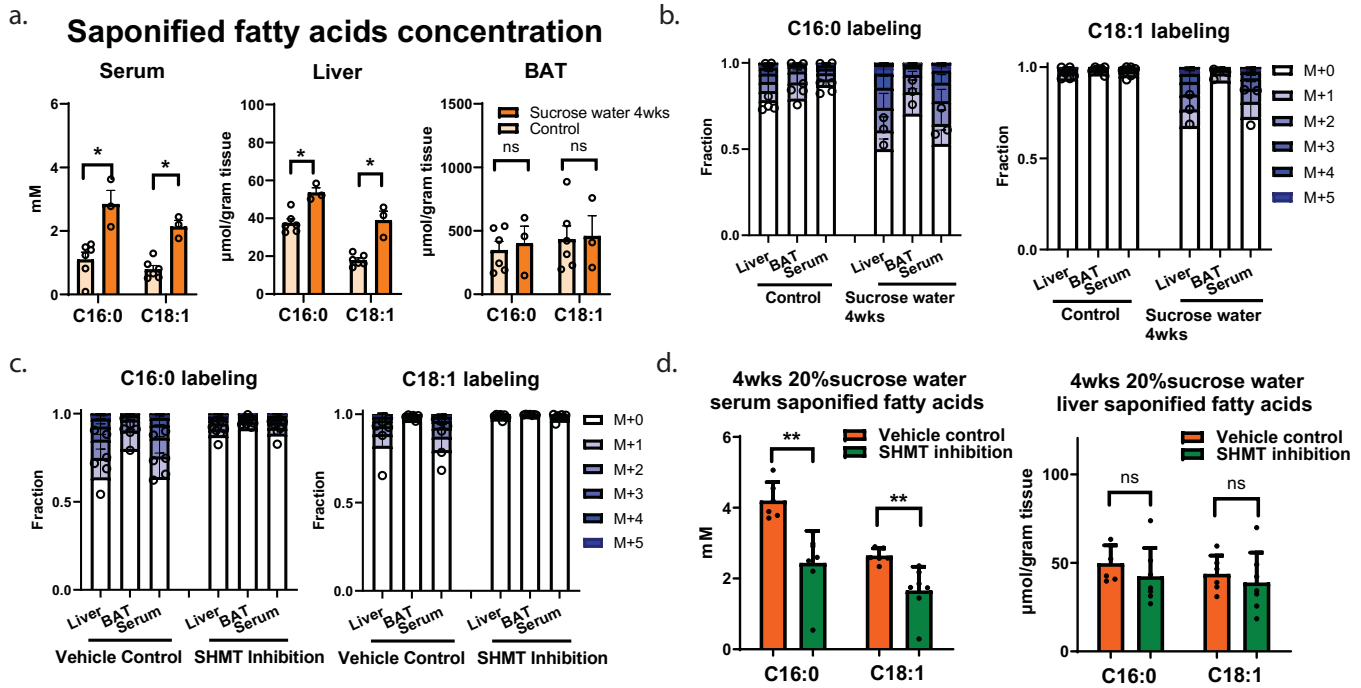

Extended Data Fig. 10 | SHMT inhibition reduced sucrose-water induced hepatic lipogenesis increase. (**a**) Saponified C16:0 and C18:1 concentration of serum, liver, and BAT in control and 4 weeks 20% sucrose water drinking mice (control vs. sucrose water drinking, serum $p = 0.024$ for C16:0, $p = 0.024$ for C18:1; liver $p = 0.024$ for C16:0, $p = 0.024$ for C18:1; BAT $p = 0.90$ for C16:0, $p = 0.99$ for C18:1.). (**b**) C16:0 and C18:1 labeling fraction in liver, brown adipose tissue, and serum from fed state 12 h D_2O infusion of control and 4 weeks 20% sucrose water drinking mice. (**c**) Saponified C16:0 and C18:1 labeling after 4 weeks 20% sucrose water drinking in liver, brown adipose tissue, and serum with or without SHIN2 treatment after 4 weeks 20% sucrose water drinking. (**d**) Overall serum and liver levels of fatty acids with or without SHIN2 treatment (control vs. SHIN2 treatment, $p = 0.0022$ for C16:0; $p = 0.0043$ for C18:1). As is (g), for liver (control vs. SHIN2 treatment, $p = 0.23$ for C16:0, $p = 0.44$ for C18:1). Mean± s.d. For experiments comparing control to sucrose water drinking, $n = 6$ for control, $n = 3$ for 4-week sucrose water drinking. For experiments comparing vehicle to SHIN2 treatment, $n = 6$ for control and $n = 7$ for SHIN2. *$p < 0.05$; **$p < 0.01$; ***$p < 0.005$ by unpaired Mann-Whitney test. All mice are males.

nature research

Corresponding author(s): Joshua.D.Rabinowitz

Last updated by author(s): Sep 10, 2021

Reporting Summary

Nature Research wishes to improve the reproducibility of the work that we publish. This form provides structure for consistency and transparency in reporting. For further information on Nature Research policies, see Authors & Referees and the Editorial Policy Checklist.

Statistics

For all statistical analyses, confirm that the following items are present in the figure legend, table legend, main text, or Methods section.

n/a	Confirmed
☐	☒ The exact sample size (*n*) for each experimental group/condition, given as a discrete number and unit of measurement
☐	☒ A statement on whether measurements were taken from distinct samples or whether the same sample was measured repeatedly
☐	☒ The statistical test(s) used AND whether they are one- or two-sided *Only common tests should be described solely by name; describe more complex techniques in the Methods section.*
☒	☐ A description of all covariates tested
☐	☒ A description of any assumptions or corrections, such as tests of normality and adjustment for multiple comparisons
☐	☒ A full description of the statistical parameters including central tendency (e.g. means) or other basic estimates (e.g. regression coefficient) AND variation (e.g. standard deviation) or associated estimates of uncertainty (e.g. confidence intervals)
☐	☒ For null hypothesis testing, the test statistic (e.g. *F*, *t*, *r*) with confidence intervals, effect sizes, degrees of freedom and *P* value noted *Give P values as exact values whenever suitable.*
☒	☐ For Bayesian analysis, information on the choice of priors and Markov chain Monte Carlo settings
☒	☐ For hierarchical and complex designs, identification of the appropriate level for tests and full reporting of outcomes
☒	☐ Estimates of effect sizes (e.g. Cohen's *d*, Pearson's *r*), indicating how they were calculated

Our web collection on statistics for biologists contains articles on many of the points above.

Software and code

Policy information about availability of computer code

Data collection	Xcalibur 4.3 (ThermoFisher, OPTON-3096) was used to collect rate mass spec data. El-Maven v12 was used to collect peak data. (https://github.com/ElucidataInc/ElMaven)
Data analysis	El-Maven v12 was used to analyze data. (https://github.com/ElucidataInc/ElMaven); Natural isotope correction was done with a published code. (https://github.com/lparsons/accucor) (PMID: 28471646); Matlab 2020a was used to do calculations following equations included in the methods section. Statistics were performed in GraphPad Prism 9.

For manuscripts utilizing custom algorithms or software that are central to the research but not yet described in published literature, software must be made available to editors/reviewers. We strongly encourage code deposition in a community repository (e.g. GitHub). See the Nature Research guidelines for submitting code & software for further information.

Data

Policy information about availability of data

All manuscripts must include a data availability statement. This statement should provide the following information, where applicable:

- Accession codes, unique identifiers, or web links for publicly available datasets
- A list of figures that have associated raw data
- A description of any restrictions on data availability

Data from figures is provided in source files. All raw data, analyzed data and materials will be provided upon request to the corresponding author (joshr@princeton.edu). We plan to also make the data available through an in-house data repository that is currently in development for easy retrieval and processing of stable isotope tracing mass spectrometry data.

Field-specific reporting

Please select the one below that is the best fit for your research. If you are not sure, read the appropriate sections before making your selection.

☒ Life sciences ☐ Behavioural & social sciences ☐ Ecological, evolutionary & environmental sciences

For a reference copy of the document with all sections, see nature.com/documents/nr-reporting-summary-flat.pdf

Life sciences study design

All studies must disclose on these points even when the disclosure is negative.

Sample size	No statistical method was used to predetermine sample size. For both in vitro and in vivo studies the number of mice were in accordance with the literature and based on previous experience in our group- in vitro PMID: 28911221, PMID: 31058257; in vivo: PMID: 32694791,PM:33472024.
Data exclusions	No data was excluded from analysis in this study.
Replication	The data represent the combined results of multiple mouse cohorts with studies performed on independent occasions. Each experiment was at least attempted twice. All attempts at replication were successful and included in this study.
Randomization	All samples were randomized during analysis.
Blinding	No blinding was implimented. Blinding for MS data analysis is not standard since data is objective and quantitative.

Reporting for specific materials, systems and methods

We require information from authors about some types of materials, experimental systems and methods used in many studies. Here, indicate whether each material, system or method listed is relevant to your study. If you are not sure if a list item applies to your research, read the appropriate section before selecting a response.

Materials & experimental systems

n/a	Involved in the study
☒	☐ Antibodies
☐	☒ Eukaryotic cell lines
☒	☐ Palaeontology
☐	☒ Animals and other organisms
☒	☐ Human research participants
☒	☐ Clinical data

Methods

n/a	Involved in the study
☒	☐ ChIP-seq
☒	☐ Flow cytometry
☒	☐ MRI-based neuroimaging

Eukaryotic cell lines

Policy information about cell lines

Cell line source(s)	HepG2 cells from ATCC.
Authentication	HepG2 cells were bought from ATCC and were not authenticated in house.
Mycoplasma contamination	Mycoplasma contanimtion has been tested negative in hepG2 cells.
Commonly misidentified lines (See ICLAC register)	No misidentified lines were used.

Animals and other organisms

Policy information about studies involving animals; ARRIVE guidelines recommended for reporting animal research

Laboratory animals	C57BL/6NCrl mice and C57BL/6 mice with SHMT1 knock-out. Both male and female mice were used and sex was indicated in figure legends. Mice were between 8 and 16 weeks old.
Wild animals	No wild animal involved.
Field-collected samples	No field-collected samples involved.

Ethics oversight	Mouse work was approved by the Princeton University Institute Animal Care and Use Committee.

Note that full information on the approval of the study protocol must also be provided in the manuscript.